Discovery of the first wide L dwarf + giant binary system and eight other ultra-cool dwarfs in wide binaries

Z.H. Zhang[1][*], D. J. Pinfield[1], A. C. Day-Jones[2,1], B. Burningham[1],
H. R. A. Jones[1], S. Yu[3], J. S. Jenkins[2], Z. Han[4,7], M. C. Gálvez-Ortiz[1],
J. Gallardo[2], A. E. García Pérez[5,1], D. Weights[1], C. G. Tinney[6], R. S. Pokorny[4,7]

[1] *Centre for Astrophysics Research, Science and Technology Research Institute, University of Hertfordshrie, Hatfield AL10 9AB, UK*
[2] *Department of Astronomy, Universidad de Chile, Casilla postal 36D, Santiago, Chile*
[3] *Armagh Observatory, College Hill, Armagh BT61 9DG, Northern Ireland, UK*
[4] *National Astronomical Observatories/Yunnan Observatory, Chinese Academy of Sciences, Kunming 650011, China*
[5] *Department of Astronomy, University of Virginia, P.O. Box 400325, Charlottesville, VA 22904-4325, USA*
[6] *School of Physics, University of New South Wales, 2050, Australia*
[7] *Key Laboratory for the Structure and Evolution of Celestial Objects, Chinese Academy of Sciences, China*

ABSTRACT

We identify 806 ultra-cool dwarfs from their SDSS *riz* photometry (of which 34 are newly discovered L dwarfs) and obtain proper motions through cross matching with UKIDSS and 2MASS. Proper motion and distance constraints show that nine of our ultra-cool dwarfs are members of widely separated binary systems; SDSS 0101 (K5V+M9.5V), SDSS 0207 (M1.5V+L3V), SDSS 0832 (K3III+L3.5V), SDSS 0858 (M4V+L0V), SDSS 0953 (M4V+M9.5V), SDSS 0956 (M2V+M9V), SDSS 1304 (M4.5V+L0V), SDSS 1631 (M5.5V+M8V), SDSS 1638 (M4V+L0V). One of these (SDSS 0832) is shown to be a companion to the bright K3 giant η Cancri. Such primaries can provide age and metallicity constraints for any companion objects, yielding excellent benchmark objects. η Cancri AB is the first wide ultra-cool dwarf + giant binary system identified. We present new observations and analysis that constrain the metallicity of η Cancri A to be near solar, and use recent evolutionary models to constrain the age of the giant to be $2.2-6.1$ Gyr. If η Cancri B is a single object, we estimate its physical attributes to be; mass = $63-82$ M_{Jup}, T_{eff} = 1800±150 K, log g = 5.3−5.5, [M/H] = 0.0±0.1. Its colours are non typical when compared to other ultra-cool dwarfs, and we also assess the possibility that η Cancri B is itself an unresolved binary, showing that the combined light of an L4 + T4 system could provide a reasonable explanation for its colours.

Key words: stars: low-mass, brown dwarfs – stars: late type – binaries: general – stars: individual (η Cancri).

1 INTRODUCTION

The number of discovered brown dwarfs is increasing rapidly (e.g., DwarfArchives.org), benefitting from optical and near-infrared large area surveys such as the Deep Near-Infrared Survey of the Southern Sky (DENIS; Epchtein et al. 1997), the Two Micron All Sky Survey (2MASS; Skrutskie et al. 2006), the Sloan Digital Sky Survey (SDSS; Abazajian et al. 2009), and the UKIRT (United Kingdom Infrared Telescope) Infrared Deep Sky Survey (UKIDSS; Lawrence et al. 2007). Ultra-cool dwarfs have red optical-near-infrared colours due to their low effective temperature. Observable ultra-cool dwarfs are nearby because of their intrinsic faintness, and can therefore have relatively higher proper motion. It is very effective to select ultra-cool dwarfs by colour (e.g. Cruz et al. 2007; Chiu et al. 2006; Zhang et al. 2009b; Pinfield et al. 2008) or proper motion (Deacon et al. 2009; Sheppard & Cushing 2009). Proper motion is also a powerful tool for identifying ultra-cool dwarf companions to other stars since such binary systems are common proper motion pairs (e.g. Burningham et al. 2009; Day-Jones et al. 2008; Luhman et al. 2007; Pinfield et al. 2006; Tokovinin et al. 2006).

[*] E-mail: zenghuazhang@hotmail.com

We generically refer to such ultra-cool dwarfs as benchmark objects, for which optimal primaries include subgiant/giant stars and white dwarfs (Pinfield et al. 2006) along with the more common main sequence primaries (Jenkins et al. 2009). Such systems are valuable, since ultra-cool dwarf properties may be constrained (at some level) by the primary star.

Current brown dwarf models have difficulty in accurately reproducing observations, and benchmark objects are thus needed to calibrate both atmospheric and evolutionary models. In order for a brown dwarf to be considered a benchmark it must have one or more properties (e.g. age, mass, distance, metallicity) that can be constrained relatively independently of ultra-cool dwarf models. The overall usefulness of an object as a benchmark is also dependent on the accuracy of the measured properties and the number of assumptions that have to be made if some degree of referencing to models is required.

The galactic disk population provides a number of host environments that are useful for the discovery of such benchmarks. Many identified benchmarks are members of young clusters such as the Hyades, Pleiades and Praesepe (Bouvier et al. 2008; Hogan et al. 2008; Casewell et al. 2007; Bihain et al. 2006; Rebolo et al. 1995; Chappelle et al. 2005; Magazzù et al. 1998; Martín et al. 1998, 1996; Zapatero Osorio et al. 1998; Cossburn et al. 1997) and moving groups (e.g. LP 944-20; Ribas 2003; Tinney 1998; Clarke et al. 2009). These kinds of benchmarks provide accurate ages and metallicities that can be inferred from other cluster/group members. However due to cluster evaporation (Bouvier et al. 2008) or disk heating mechanisms (De Simone et al. 2004), the spatial concentrations become dispersed and kinematic signatures diffused after $\sim$1 Gyr. Such benchmarks thus only populate the <1 Gyr age range, and are not fully applicable for studies of brown dwarf evolution across the full age extent of the galactic disk. This is also the case for isolated field brown dwarfs that have Lithium in their atmospheres, such as DENISp-J1228.2-1547 (Delfosse et al. 1997; Tinney et al. 1997), SDSSJ0423-0414 (Burgasser et al. 2005), 2M0850 (Kirkpatrick et al. 1999) and Kelu1 (Ruiz et al. 1997), where the Lithium test can be used to estimate their age (Magazzù et al. 1993).

More useful for this purpose are brown dwarfs as members of binaries, where the host star can provide age, distance and in some cases metallicity constraints. How useful these systems are is dependent on how well we understand the nature and physics of the primary stars. Main sequence star ages can be largely uncertain due to the degeneracy of evolutionary models on the main-sequence (e.g. Girardi et al. 2000; Yi et al. 2001). Tighter age constraints can be gained from more evolved stars, e.g. subgiants, giants and white dwarfs. Such primaries can constrain accurate ages, as well as metallicity in the case of subgiants and early phase giant stars, via robust models. These types of binary systems can populate the full age range of the disk up to 10 Gyrs (see Pinfield et al. 2006).

Benchmark brown dwarfs can also be in brown dwarf + brown dwarf binary pairs where the dynamical mass of the components can be calculated. Liu et al. (2008a) suggest that these systems will yield good determinations of gravity and age. However they cannot, in general provide accurate metallicity estimations, except for the rare examples that are found to be members of a cluster or components of a higher multiple system (where a higher mass component has known metallicity), as is the case for HD 10948BC (Dupuy et al. 2009).

In this paper we report the discovery of nine common proper motion binary systems with ultra-cool dwarf components. One is a benchmark L dwarf companion to the giant star η Cancri, and the other eight are late M and early L dwarf companions to K-M dwarf stars. The photometric selection processes are presented in Section 2. The spectral types are presented in Section 3. Distances are presented in Section 4. Proper motions are presented in Section 5. η Cancri AB is presented and discussed in Section 6, and Section 7 presents a summary.

2   PHOTOMETRIC SELECTION

2.1   SDSS identification

The SDSS uses a dedicated 2.5 m telescope equipped with a large format mosaic CCD camera to image the sky in five optical bands (u, g, r, i, z), and two digital spectrographs to obtain the spectra of galaxies, quasars and late type stars selected from the imaging data (York et al. 2000). The SDSS magnitude limits (95% detection repeatability for point sources) for the u, g, r, i and z bands are 22.0, 22.2, 22.2, 21.3 and 20.5 respectively, all magnitudes are in SDSS AB system (Adelman-McCarthy et al. 2008).

The SDSS $i - z$ colour is particularly useful for L dwarf selection (Fan et al. 2000). We used $2 < i - z < 3.2$ in our previous ultra-cool proper motion work (Zhang et al. 2009b) to select L dwarf candidates. In this work, we focus on a bluer sample to increase our sample size and increase the fraction of objects that have measured SDSS spectra. We used $1.5 < i - z < 2$ and $1.5 < r - i < 4.5$ for objects with SDSS spectra, leading to a total ultra-cool dwarf sample of 3154 objects. For objects without spectra we used a more constraining selection, requiring $1.7 < i - z < 2, 2 < r - i < 3.3, r - i < 7(i - z) - 9.3, 16 < z < 19.5$, and $17 < i < 21.2$. Figure 1 shows the colour criteria for these selections.

We also made a deeper ultra-cool dwarf search towards the young open cluster Praesepe (M44; age = 0.79 Gyr, d = 181.5 pc; van Leeuwen 2009). The original motivation was to identify faint cluster members, however the most interesting discovery from this search was a foreground field object (see Section 5.2), so we have chosen to present the analysis of this deeper search here, along with that of our shallower search in the field. The Praesepe cluster has been surveyed by SDSS and UKIDSS (the Galactic Cluster Survey, within $3°$ of 08h40m06s,$+19°41'06''$), and we used the same colour criteria as previously described for SDSS objects without spectra. However, the original aim to identify ultra-cool dwarfs at the distance of the cluster (e.g. van Leeuwen 2009; Taylor 2006) led us to limit this search to $19 < z < 20.5$ and $21 < i < 22.4$, corresponding to early L dwarfs ($i - z = 1.8-2.1$; Zhang et al. 2009b) at $\sim$100$-$200 pc (see the $M_i - (i - z)$ spectral type relationship (Hawley et al. 2002)).
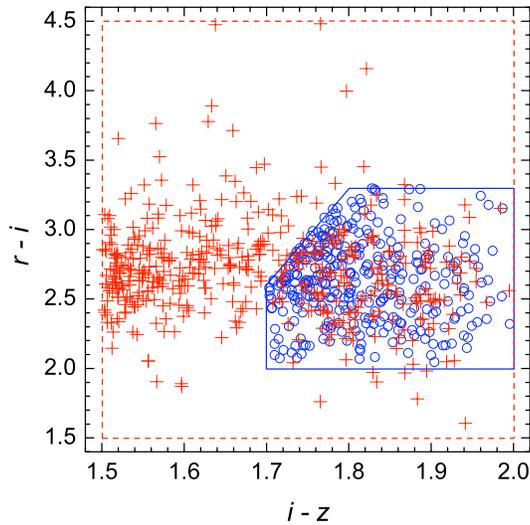
Figure 1. *riz* colour space for ultra-cool dwarfs with (*red crosses*) and without (*blue circles*) SDSS spectra. The *polygons* show the *r-i* and *i-z* colour limits used to select ultra-cool dwarfs with (*red dashed lines*) and without (*blue solid lines*) spectra.

2.2 Near-infrared photometry

Near-infrared colours provide additional information useful for spectral typing ultra-cool dwarfs. SDSS selected candidates were cross matched with point sources in the 2MASS (Cutri et al. 2003) and UKIDSS (Lawrence et al. 2007) catalogues. We used a matching radius of 6″ to ensure that ultra-cool dwarfs with high proper motion would generally be matched by this procedure, despite possible motion over a period of up to ∼8 years (between SDSS-2MASS, and SDSS-UKIDSS epochs). 563 objects with spectra were cross matched in SDSS and 2MASS, of which 469 were also cross matched in UKIDSS. 1761 objects without spectra were cross matched in SDSS and 2MASS, of which 337 objects were cross matched in UKIDSS. So 806 SDSS objects (see online material Table 9 for these ultra-cool dwarfs) were cross matched in 2MASS and UKIDSS of which 469 objects have SDSS spectra. For our ultra-cool dwarf sample towards Praesepe, we cross matched candidates with the UKIDSS Galactic Cluster Survey (GCS), which covers 28 square degrees of the cluster (radius ∼3°) in *ZYJHK*.

## 3 SPECTRAL TYPES

3.1 SDSS red optical spectroscopy

The SDSS imaging data are used to uniformly select different classes of objects whose spectra will be taken with the SDSS 2.5 m telescope (York et al. 2000). The target selection algorithms for spectroscopic follow up are described by Stoughton et al. (2002). The wavelength coverage is from 3800 to 9200 Å with a resolving power $\lambda/(\Delta\lambda) = 1800$. The signal-to-noise ratio is better than 4 pixel^{-1} at $g = 20.2$ (Adelman-McCarthy et al. 2008). SDSS spectra have been
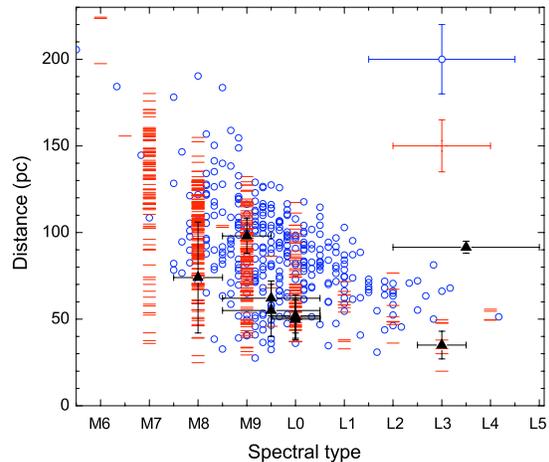
Figure 3. Plot of distance vs. spectral type for ultra-cool dwarfs identified with SDSS spectra (*red bars*) and optical-infrared colours (*blue circles*). Typical errors in spectral type and distance are shown in the top right. *Black triangles* and the black *square* (SDSS 0832) are the objects subsequently found to be in common proper motion binary systems (see Section 5.3). For these companions we assume their distances are the same as their primary stars (see Section 5.3).

sky subtracted and corrected for telluric absorption. The spectroscopic data are automatically reduced by the SDSS pipeline software. For 469 ultra-cool dwarf candidates with SDSS spectra, we assigned their spectral type with the HAMMER pipeline (Covey et al. 2007). The typical spectral type error is ∼0.5−1.0 subtypes. A comparison between our analysis and the literature (Reid et al. 2008; West et al. 2008; Cruz et al. 2007, 2003; Kendall et al. 2007; Hawley et al. 2002; Schneider et al. 2002; Kirkpatrick et al. 2000) shows generally good agreement, with a small number of minor ambiguities. These are 79 L dwarfs with SDSS spectra in our sample, 11 objects are known L dwarfs (one of them is in binary system), 42 objects are catalogued by West et al. (2008) as M9 or L0 dwarfs and 34 new L dwarfs are presented. Table 1 shows the SDSS, 2MASS and UKIDSS photometric data of the 34 new L dwarfs. Figure 2 shows the SDSS spectra of 39 ultra-cool dwarfs. SDSS name and spectral types are labeled. The six ultra-cool dwarfs that we subsequently found to be wide binary companions (see Section 5.3) are labeled with both their original name and their new binary name.

Of these companion ultra-cool dwarfs, SDSS J020735.59+135556.2 (SDSS 0207) was characterized by Hawley et al. (2002) as an L3 dwarf using its SDSS spectrum, and SDSS J085836.97+271050.8 (SDSS 0858), SDSS J095613.13+014514.3 (SDSS 0956), SDSS 163817.31+321144.1 (SDSS 1638) and SDSS 163126.15+294836.9 (SDSS 1631) were catalogued by West et al. (2008) as an L0, L0, M9 and M8 respectively. The spectra of these previously identified ultra-cool dwarfs are shown in blue. The spectra of SDSS 130433.16+090706.9 (SDSS 1304), a new L0 dwarf companion, and the other 33 new L dwarfs discovered in this work are shown in black.
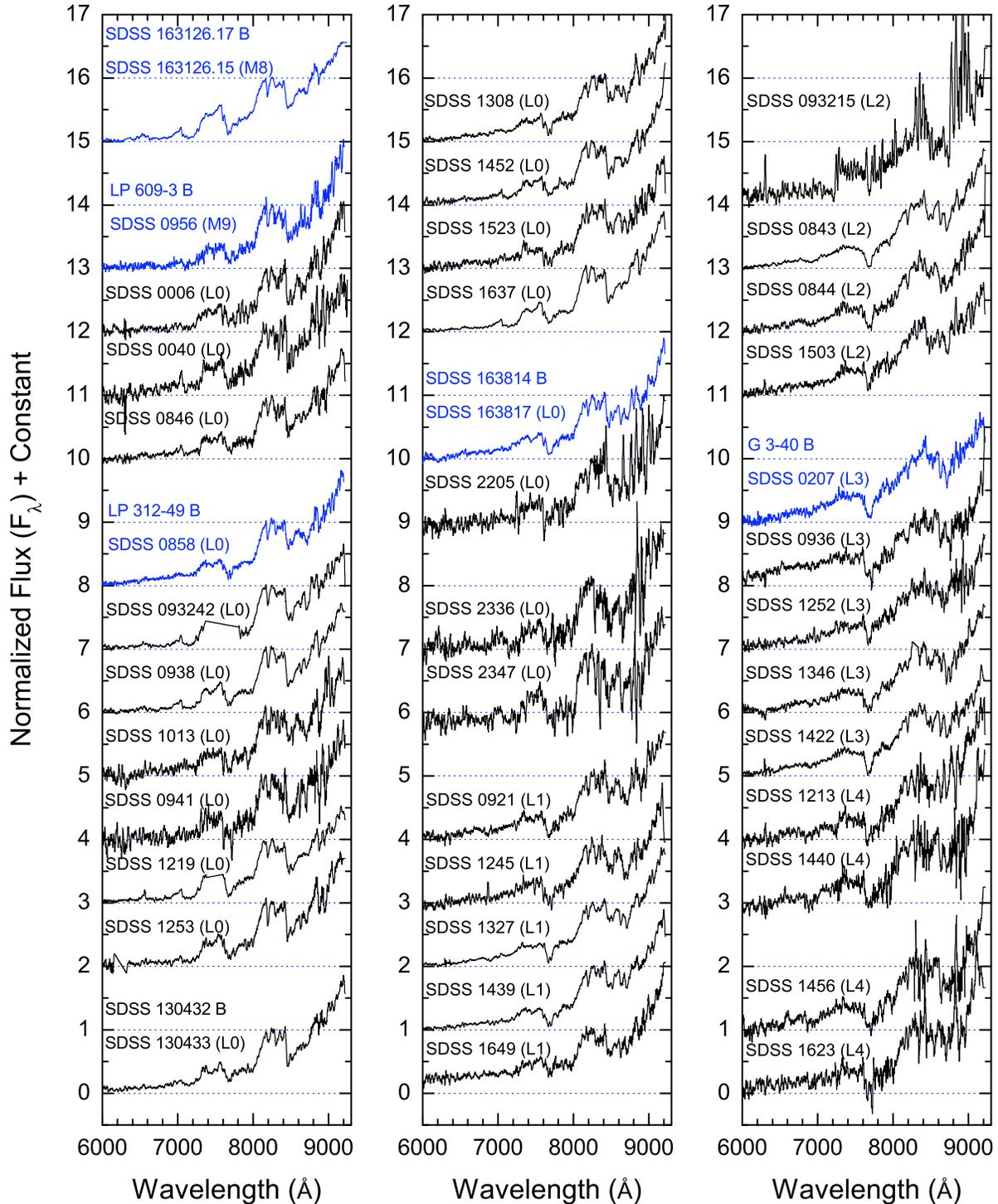
Figure 2. SDSS spectra of 39 ultra-cool dwarfs. Six objects in binary systems are those with two names (see Section 5.3), of which five are previously identified ultra-cool dwarfs (*blue*). The remaining 34 objects (*black*) are new L dwarfs discovered in this work, one of which is in a binary system. Note that two of the binaries we present in this paper do not have spectroscopy at this time. All spectra have been normalized to one at 8250 Å, smoothed by 11 pixels, and vertically offset for clarity. *Dotted lines* indicate Zero point offsets and also normalization levels to aid the visual examination of spectra.

Table 1. Photometric data of 34 new L dwarfs.

Name	SDSS i	SDSS z	2MASS J	2MASS H	2MASS K	UKIDSS Y	UKIDSS J	UKIDSS H	UKIDSS K	Sp.Type
SDSS J000614.06+160454.5	20.74±0.06	18.92±0.05	16.59±0.13	15.84±0.11	15.09±0.16	...	...	15.88±0.02	15.32±0.02	L0
SDSS J004058.92+152845.0	20.59±0.06	18.85±0.04	16.96±0.21	15.58±0.15	15.60±0.23	...	...	15.96±0.02	15.48±0.02	L0
SDSS J084333.28+102443.5	19.30±0.02	17.46±0.01	14.87±0.04	14.09±0.04	13.67±0.04	15.99±0.01	14.78±0.01	14.10±0.01	13.55±0.01	L2
SDSS J084407.00+284702.1	20.17±0.04	18.25±0.03	15.87±0.06	14.82±0.05	14.34±0.06	15.76±0.01	...	...	...	L2
SDSS J084610.73+030837.5	20.29±0.04	18.39±0.03	15.91±0.09	15.17±0.10	15.03±0.17	16.95±0.01	...	15.29±0.01	14.76±0.01	L0
SDSS J092142.51+084202.7	19.56±0.04	17.82±0.03	15.79±0.08	14.89±0.09	14.34±0.07	16.80±0.01	15.65±0.01	15.00±0.01	...	L1
SDSS J093215.45+345624.8	20.60±0.04	18.81±0.03	16.73±0.15	15.70±0.14	14.98±0.14	...	16.34±0.01	...	...	L2
SDSS J093242.84+042215.2	19.55±0.02	17.87±0.02	15.66±0.08	14.91±0.07	14.62±0.09	...	...	15.00±0.01	14.51±0.01	L0
SDSS J093600.12+043147.9	20.86±0.07	18.98±0.04	16.12±0.09	15.13±0.06	14.48±0.09	...	...	15.20±0.01	14.44±0.01	L3
SDSS J093858.87+044343.9	19.23±0.02	17.50±0.02	15.24±0.05	14.50±0.05	14.00±0.07	...	...	14.59±0.01	14.02±0.01	L0
SDSS J094140.65−003215.8	20.60±0.05	18.79±0.04	16.77±0.12	15.99±0.14	15.59±0.21	17.49±0.02	16.69±0.02	16.30±0.02	15.86±0.02	L0
SDSS J101304.34+071050.7	20.51±0.04	18.62±0.03	16.22±0.14	15.47±0.14	15.09±0.18	17.22±0.02	16.19±0.01	15.60±0.01	15.07±0.01	L0
SDSS J121304.77+152922.2	20.69±0.07	18.76±0.05	16.33±0.11	15.66±0.12	15.42±0.16	...	...	15.69±0.02	15.18±0.02	L4
SDSS J121917.86+151612.4	19.46±0.02	17.88±0.02	15.68±0.07	15.09±0.08	14.71±0.11	...	...	15.08±0.01	14.62±0.01	L0
SDSS J124514.95+120442.0	20.53±0.04	18.67±0.03	16.05±0.08	15.32±0.11	14.73±0.09	17.14±0.02	16.06±0.01	15.33±0.01	14.67±0.01	L1
SDSS J125214.08+142239.3	20.56±0.04	18.76±0.04	16.00±0.07	15.16±0.08	14.49±0.07	17.28±0.02	16.05±0.01	15.24±0.01	14.58±0.01	L3
SDSS J125331.83+065933.4	20.20±0.04	18.35±0.03	16.19±0.11	15.27±0.10	15.07±0.16	17.01±0.01	16.07±0.01	15.48±0.01	14.96±0.01	L0
SDSS J130433.16+090706.9[a]	19.11±0.02	17.33±0.02	15.29±0.06	14.57±0.07	13.95±0.07	16.32±0.01	15.28±0.01	14.59±0.01	14.03±0.01	L0
SDSS J130831.02+081852.3	19.60±0.02	17.82±0.02	15.13±0.05	14.35±0.06	13.85±0.07	16.31±0.01	15.19±0.01	14.37±0.01	13.79±0.01	L0
SDSS J132715.21+075937.5	19.17±0.02	17.33±0.01	14.60±0.04	13.79±0.04	13.24±0.04	15.75±0.01	14.58±0.01	13.83±0.01	13.20±0.01	L1
SDSS J134607.41+084234.5	20.04±0.03	18.16±0.02	15.74±0.07	14.79±0.08	14.16±0.07	16.74±0.01	15.52±0.01	14.75±0.01	14.11±0.01	L3
SDSS J142257.14+082752.1	19.37±0.02	17.60±0.02	15.10±0.05	14.22±0.03	13.65±0.05	16.24±0.01	15.01±0.01	14.27±0.01	13.61±0.01	L3
SDSS J143911.87+082315.6	19.84±0.03	17.93±0.02	15.39±0.04	14.65±0.05	14.09±0.07	16.54±0.01	15.35±0.01	14.69±0.01	14.09±0.01	L1
SDSS J144016.19+002638.9	20.43±0.05	18.57±0.03	16.07±0.11	15.41±0.12	14.82±0.14	17.21±0.02	16.01±0.01	15.28±0.01	14.69±0.01	L4
SDSS J145201.33+093136.8	19.69±0.02	17.79±0.02	15.42±0.07	14.77±0.08	14.25±0.09	16.35±0.01	15.34±0.01	14.81±0.01	14.28±0.01	L0
SDSS J145658.17+070104.7	20.55±0.04	18.66±0.03	16.28±0.11	15.20±0.09	14.60±0.10	17.24±0.01	15.97±0.01	15.25±0.01	14.59±0.01	L4
SDSS J150309.53+115323.1	20.68±0.04	18.74±0.04	16.30±0.10	15.40±0.10	14.79±0.09	17.32±0.01	16.14±0.01	15.42±0.01	14.80±0.01	L2
SDSS J152314.46+105258.9	20.53±0.04	18.57±0.03	16.09±0.10	15.15±0.08	14.82±0.12	17.08±0.01	15.94±0.01	15.20±0.01	14.62±0.01	L0
SDSS J162307.37+290827.6	20.38±0.05	18.50±0.04	16.08±0.09	15.50±0.11	14.97±0.10	...	16.13±0.01	...	...	L4
SDSS J163748.64+275254.6	19.01±0.02	17.29±0.01	14.95±0.04	14.16±0.05	13.84±0.05	...	14.89±0.01	...	...	L0
SDSS J164911.16+300048.3	20.26±0.03	18.38±0.03	16.12±0.09	15.38±0.11	14.92±0.09	...	16.09±0.01	...	...	L1
SDSS J220517.48−003710.3	21.02±0.06	19.13±0.05	16.82±0.14	16.24±0.20	15.46±0.19	17.79±0.03	...	15.98±0.02	15.52±0.02	L0
SDSS J233615.99+004253.4	20.94±0.07	19.05±0.04	17.08±0.20	15.71±0.14	15.29±0.16	17.59±0.02	16.63±0.02	15.98±0.02	15.37±0.02	L0
SDSS J234759.77−001546.9	20.86±0.07	19.10±0.06	16.40±0.13	16.15±0.20	15.46±	17.77±0.02	16.90±0.02	16.31±0.03	15.88±0.03	L0

Note: SDSS magnitude limits (95% detection repeatability for point sources) for i and z bands are 21.3 and 20.5 respectively; UKIDSS magnitude limits for Y, J, H and K bands are 20.5, 20.0, 18.8 and 18.4 respectively.

[a] Companion to an M4.5 dwarf, SDSS J130432.93+090713.7, see Table 4.

3.2   Spectral types from colours

We used optical−near-infrared colour−spectral type relationships (Zhang et al. 2009a,b) to assign the spectral types of 337 objects without SDSS spectra. More specifically, we used three spectral type−colour (i-J, i-H, i-K) relationships, and took the average value of the three results. The typical error of the spectral type is about ±1.5 subtypes. Figure 3 shows the spectral types of the ultra-cool dwarfs from both typing methods (as well as their distance estimates; see Section 4).

3.3   Near-infrared spectral type

Spectroscopy in the J-band was obtained for ULAS 0832 using the Near InfraRed Imager and Spectrometer (NIRI; Hodapp et al. 2003) on the Gemini North Telescope on Mauna Kea (under program GN-2009A-Q-16) on the 8th of April 2009 through thin cirrus cloud. All observations were made up of a set of sub-exposures in an ABBA jitter pattern to facilitate effective background subtraction, with a slit width of $1''$. The length of the A-B jitter was $10''$, and the integration consisted of 6 sub-exposures of 240 seconds.

The NIRI observations were reduced using standard IRAF Gemini packages. A comparison argon arc frame was used to obtain a dispersion solution, which was applied to the pixel coordinates in the dispersion direction on the images. The resulting wavelength-calibrated subtracted AB-pairs had a low-level of residual sky emission removed by fitting and subtracting this emission with a set of polynomial functions fit to each pixel row perpendicular to the dispersion direction, and considering pixel data on either side of the target spectrum only. The spectra were then extracted using a linear aperture, and cosmic rays and bad pixels removed using a sigma-clipping algorithm.

Telluric correction was achieved by dividing the extracted target spectra by that of the F6V star HIP 41187, observed just before the target. Prior to division, hydrogen lines were removed from the standard star spectrum by interpolating the stellar continuum. Relative flux calibration was then achieved by multiplying through by a blackbody spectrum with $T_{eff} = 6300$K.

Figure 4 shows this spectrum and three standard spectra (L0, L3 and L7). The spectrum is somewhat noisy, but it but is consistent with early L spectral type by the near-infrared characterization scheme of Geballe et al. (2002).

4   DISTANCES

We used the M_J−spectral type relationship and $M_i − (i−J)$ relationship of Hawley et al. (2002) to estimate distances of ultra-cool dwarfs with and without SDSS spectra respectively. We have assumed two limiting cases. Firstly we assume that the ultra-cool dwarfs are single objects (these are the distances shown in Figure 3 and refered to as "Dist" in the subsequent tables). However, to provide conservative upper limits we also perform the calculations assuming that each candidate is an unresolved equal-mass binary giving distances 41% larger (referred to as Dist.b in subsequent tables). In each case the uncertainties were calculated to allow
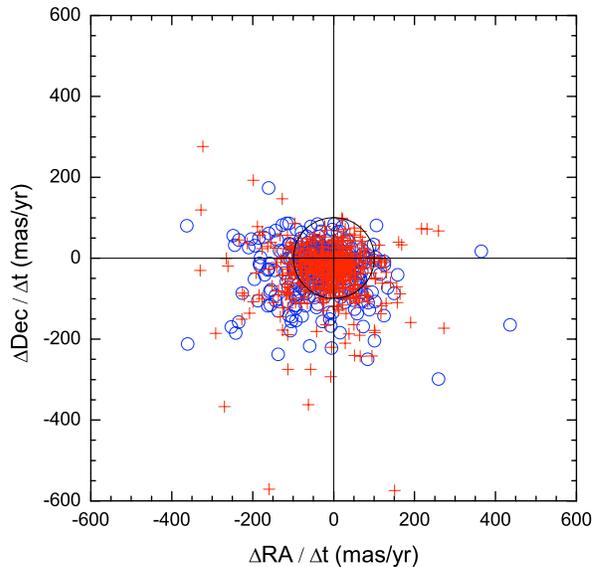
Figure 5. 2MASS-UKIDSS proper motions of ultra-cool dwarfs identified with (*red crosses*) and without (*blue circles*) SDSS spectra. A ring indicates the 100mas/yr proper motion locus, which is a useful division when searching for common proper motion companions (see text).

for spectral type uncertainty and the RMS scatter in the absolute magnitude−spectral type/colour relationships.

5   PROPER MOTIONS

In previous work by our group we have measured proper motions using various combinations of survey databases (Zhang et al. 2009b) and found that 2MASS and UKIDSS generally provide the most accurate proper motions due to longer baselines (5−10 years). The combinations of SDSS-2MASS and SDSS-UKIDSS only sometimes provide useful proper motions, when for example the baselines involved are relatively long ($\gtrsim$ 5 years) or the measured objects have large proper motions (Deacon et al. 2009; Sheppard & Cushing 2009; Zhang et al. 2009b).

5.1   Ultra-cool dwarfs from our SDSS/2MASS/UKIDSS sample

806 of our objects matched in 2MASS and UKIDSS, so we calculated proper motions from their database coordinates and epochs, following the method described in Zhang et al. (Section 3; 2009b). Figure 5 shows the resulting 2MASS-UKIDSS proper motions of these 806 ultra-cool dwarfs. The 100mas/yr ring shown in the Figure 5 acts as a guide to identify ultra-cool dwarfs whose proper motions are comparable with those in existing high proper motion catalogues (>100mas/yr). This separation is useful when searching for possible companions (see Section 5.3). Table 2 shows the proper motions and distance estimates for the 34 new L dwarfs.
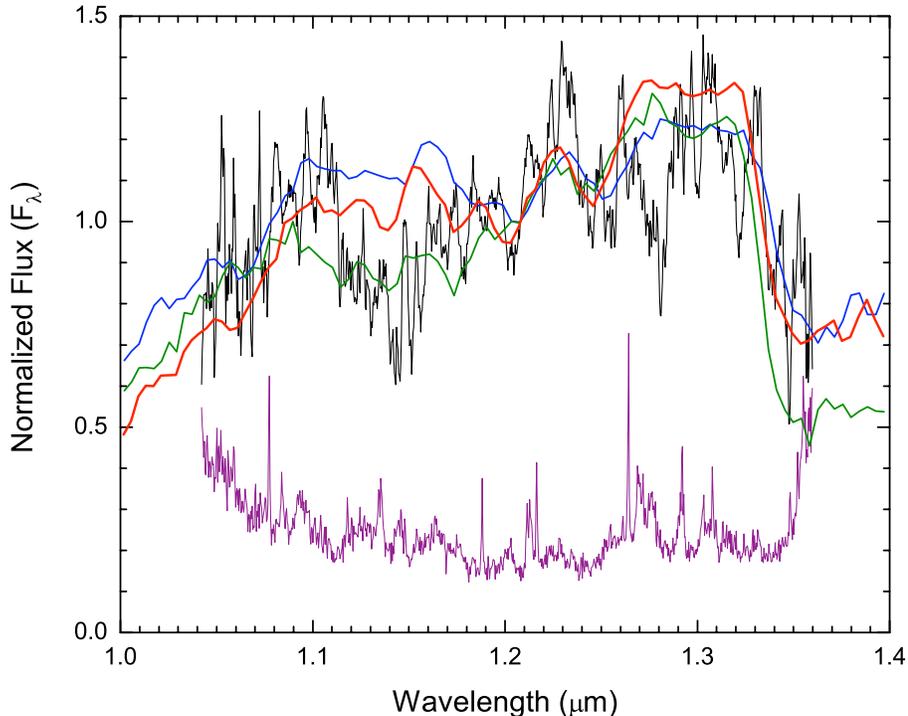
Figure 4. Gemini/NIRI spectrum of SDSS 0832. The spectrum (*black*) is normalized to one at 1.208 μm and smoothed by 11 pixels. The error spectrum is plotted in *purple*. Three standard near-infrared spectra are over plotted, 2MASP J0345432+254023 (*blue*, L0 in optical, L1 in near-infrared; Burgasser & McElwain 2006; Kirkpatrick et al. 1999), 2MASSW J1146345+223053 (*red*, L3; Burgasser et al. 2010; Kirkpatrick et al. 1999; Knapp et al. 2004), and DENIS-P J0205.4-1159 (*green*, L7 in optical, L5.5 in near-infrared; Burgasser et al. 2010; Kirkpatrick et al. 1999).

5.2 Ultra-cool dwarfs from our deeper search towards Praesepe

Due to the relatively short baselines between the SDSS and UKIDSS observations of our ultra-cool dwarfs towards Praesepe, and their low optical signal-to-noise, we obtained additional epoch imaging for some of our candidates. z-band images were obtained for two candidates, SDSS J083823.69+164702.0 (SDSS 0838) and SDSS J083231.78+202700.0 (SDSS 0832), using the ESO Faint Object Spectrograph and Camera (v.2) (EFOSC2; Buzzoni et al. 1984) on the New Technology Telescope (NTT) on La Silla, ESO (under program 082.C-0399B) on 25th December 2008 with an exposure time of 500 seconds. The EFOSC2 observations were reduced using standard IRAF packages. We then used the IRAF task GEOMAP to derive spatial transformations from the SDSS z or UKIDSS GCS K-band images into the NTT z-band images. These transforms allowed for linear shifts and rotation. We then transformed the SDSS or GCS pixel coordinates of objects into the NTT images using GEOXYTRAN, and calculated the change in position (relative to the reference stars) between the two epochs.

We measured the proper motion of SDSS 0838 (μ_{RA} = -21 ± 15 mas/yr, μ_{Dec} = -19 ± 15 mas/yr; 2.2 year baseline) based on GCS and NTT images with a baseline of 2.2 years and using 14 reference stars. This data does not yield a proper motion that is greater than zero at a strongly significant level, although we note that the measurement is potentially consistent with the proper motion of Praesepe (μ_{RA} = -35.81 mas/yr, μ_{Dec} = -12.85 mas/yr; van Leeuwen 2009). The distance constraint for SDSS 0838 (see Section 4; 181±62 pc if single, or 256±62 pc if an unresolved equal-mass binary) is also consistent with that of the cluster (181.5 pc; van Leeuwen 2009). A longer base-line is needed before cluster membership can be rigorously assessed, but this object could be a member of Praesepe. Table 5 shows the parameters of SDSS 0838.

We measured the proper motion of SDSS 0832 (μ_{RA} = -46.6 ± 8.2 mas/yr, μ_{Dec} = -37.0 ± 8.2 mas/yr) based on SDSS and NTT images with a baseline of 4.7 years and using 16 reference stars. In addition, the combination of SDSS and UKIDSS GCS epochs provided a proper motion (μ_{RA} = -52 ± 46 mas/yr, μ_{Dec} = -50 ± 46 mas/yr) with a baseline of 2.6 years (Zhang et al. 2009b) with significantly larger uncertainties. We combined these two measurements together, weighting by their reciprocal uncertainties, to give a final proper motion of μ_{RA} = -47.4 ± 8.2 mas/yr, μ_{Dec} = -38.9 ± 8.2 mas/yr for SDSS 0832. Both this proper motion and the distance constraint for SDSS 0832 (121±33 pc) are
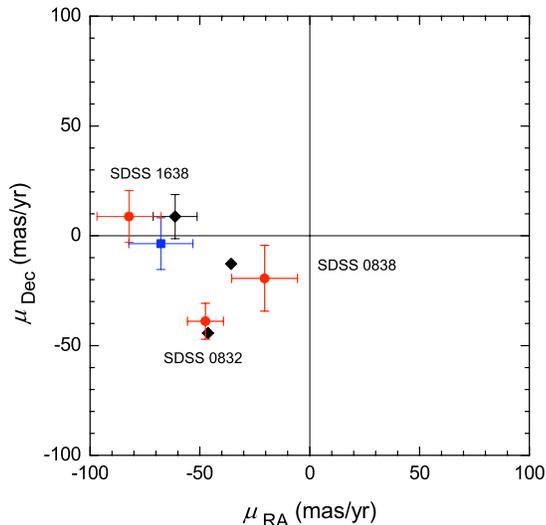
Figure 6. The proper motions of SDSS 0832 (L3.5), SDSS 0838 (M9.5), SDSS1638 (L0) and their primary star or cluster (*squares* and a *diamond* respectively). The proper motions of these three ultra-cool dwarfs (*red circles*) and the primary star of SDSS 1638 (*blue sqrare*) are measured with the IRAF routines GEOMAP and GEOXYTRAN. The *black diamonds* are proper motions from the literature. SDSS 0832 is the companion to the K3 giant η Cancri. SDSS 0838 is a Praesepe candidate member. SDSS 1638 is a companion to an M4 dwarf.
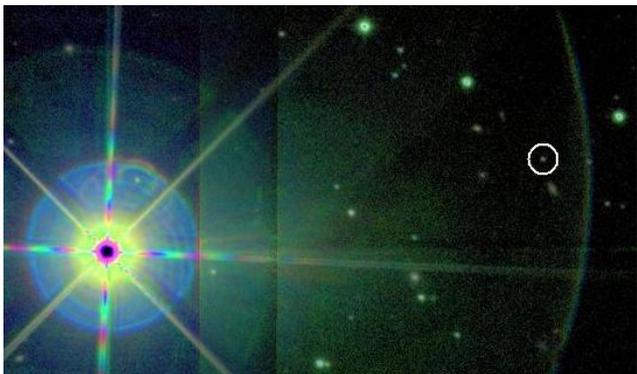
Figure 7. A UKIDSS *JHK* false colour image of η Cancri AB with a separation of 164 arcsec. η Cancri A is the brightest object in this field, η Cancri B is in the white circle.

inconsistent with the Praesepe cluster, and this ultra-cool dwarf is thus seen to be a foreground object in the field.

5.3   Common proper motion systems

We searched for common proper motion companions to our ultra-cool dwarfs using three methods that combine efficacy with efficiency. Our searches are not fully complete, but are productive and effective in the identification of companions.

For our sample of 271 objects with proper motions larger than 100 mas/yr, we searched for common proper motion companions in high proper motion catalogues (Lépine
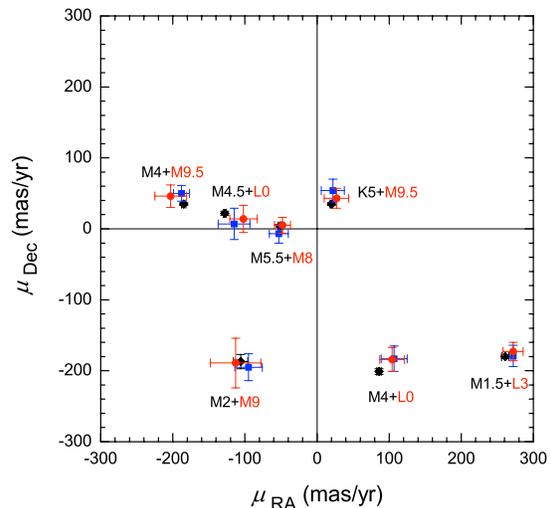
Figure 8. Seven dwarf star+ultra-cool dwarf common proper motion pairs. Proper motions of ultra-cool dwarfs (*red circles*) and dwarf stars (*blue squares*) are measured in this work using 2MASS and UKIDSS database coordinates and epochs. Dwarf star proper motions taken from the literature (*black diamonds*) are also shown.

& Shara 2005; Ivanov 2008) out to $3'$ separation, which corresponds to separation <9000 AU for closer objects (50 pc) and <27000 AU for more distant objects (150 pc), and avoids an excess of contamination through chance alignments (see Section 5.4). Four of the ultra-cool dwarfs with proper motions greater than 100 mas/yr were found to have common proper motion companions (allowing for astrometric uncertainties), and the distance constraints for each pair were consistent with shared distance. Three of these four objects have SDSS spectra (SDSS 0207, SDSS 0858 and SDSS 0956) and one [SDSS J095324.54+052658.4 (SDSS 0953)] does not.

We also conducted a systematic searched for companions to our lower proper motion (<100mas/yr) objects. This search was conducted by visiual inspection of the region of sky around each of our lower proper motion ultra-cool dwarfs using the SDSS Navigate Tool. We inspected images covering separations out to $2'$ on the sky, and looked for objects that could be mid K to mid M companions ($r - i \sim 0.5$-2.0, $i - z \sim 0.2$-1.0) with distances comparable to our sample (~ 30-150pc), and thus magnitude of $i \sim 9$-17. We then measured the proper motions of all such possible companions (as described in Section 5) to test for companionship. In this way, another four objects were found to have nearby common proper motion companions with reasonable distance agreement, three of which have SDSS spectra (SDSS 1304, SDSS 1631, SDSS 1638) and one of which [SDSS 010153.11+152819.4 (SDSS 0101)] does not.

In addition, we performed a wider angle visual search for bright companions to the two faint low proper motion ultra-cool dwarfs towards Praesepe, out to $3'$separation. This resulted in the identification of a bright giant star (η Cancri) $164''$ away from SDSS 0832. The proper motion of η

Table 3. Proper motions of companions of eight dwarf + ultra-cool dwarf binary systems.

Primary	TYC 1189-1216-1		G 3-40		LP 312-49		LP 548-50	
Ref.[a]	μ_{RA} (mas/yr)	μ_{Dec} (mas/yr)	μ_{RA} (mas/yr)	μ_{Dec} (mas/yr)	μ_{RA} (mas/yr)	μ_{Dec} (mas/yr)	μ_{RA} (mas/yr)	μ_{Dec} (mas/yr)
1	...	...	259 ...	−188 ...	...	...	...	...
2	...	...	...	...	113 ...	−196 ...	−184 ...	32 ...
3	20±3	35±3	...	...	...	...	...	...
4	21±3	35±3	261±15	−165±15	...	...	...	...
5	18 ...	34 ...	254±4	−176±1	80±1	−198±3	−182±3	36±2
6	...	...	261±6	−185±6	81±6	−205±6	...	...
7	20±2	35±2	263±2	−180±2	83±4	−202±5	−182±3	36±2
8	20±2	33±2	262 ...	−186 ...	82 ...	−201 ...	...	...
9	...	...	262 ...	−186 ...	82 ...	−201 ...	−186 ...	37 ...
10	22±1	37±1	265±2	−181±2	...	...	...	...
11	...	...	256±3	−176±3	81±3	−200±3	−191±3	36±3
12	20 ...	35 ...	264 ...	−180 ...	83 ...		...	...
13	21±1	36±1	264±3	−179±3	...	...	...	...
14	22±16	54±16	272±15	−179±15	107±18	−183±18	−188±11	50±11
Average[b]	20±2	37±2	262±2	−179±2	89±6	−199±3	−186±3	38±3
Secondary[c]	27±17	43±14	273±19	−174±17	104±20	−184±20	−203±17	46±17

Primary	LP 609-3		SDSS J130432.93+090713.7		SDSS J163126.17+294847.1		SDSS J163814.32+321133.5	
Ref.[a]	μ_{RA} (mas/yr)	μ_{Dec} (mas/yr)	μ_{RA} (mas/yr)	μ_{Dec} (mas/yr)	μ_{RA} (mas/yr)	μ_{Dec} (mas/yr)	μ_{RA} (mas/yr)	μ_{Dec} (mas/yr)
2	−105	−182	...	...	...	...	...	...
5	...	...	−126±1	22±3	−52±20	6±1	−60±1	2 ...
7	...	...	−126±1	22±3	−52±20	6±1	−60±1	2 ...
8	−107 ...	−189 ...	...	...	...	...	...	...
9	−107 ...	−189 ...	...	...	...	...	...	...
11	...	...	−132±3	22±3	−49±3	1±3	−66±3	3±3
14	−95±19	−195±19	−115±22	7±22	−53±13	−7±13	−85±10	2±10
15	...	...	...	...	...	...	−68±15	−4±12
Average[b]	−104±14	−189±19	−125±3	18±4	−52±3	2±4	−66±6	6±5
Secondary[c]	−113±37	−190±36	−102±19	14±19	−48±11	5±11	−82±15	9±12

[a] Reference: [1]Giclas et al. (1971), [2]Luyten & Hughes (1980), [3]Hog et al. (2000), [4]Kharchenko (2001), [5]Monet et al. (2003), [6]Salim & Gould (2003), [7]Zacharias et al. (2004), [8]Zacharias et al. (2009), [9]Lépine & Shara (2005), [10]Ducourant et al. (2006), [11]Adelman-McCarthy et al. (2008), [12]Ivanov (2008), [13]Röser et al. (2008), [14]measured with database information in this work, [15]measured with IRAF in this work.

[b] Average proper motions of primary stars.

[c] Proper motions of secondary ultra-cool dwarfs.

Cancri ($\mu_{RA} = -46.33\pm0.43$ mas/yr, $\mu_{Dec} = -44.31\pm0.24$ mas/yr) is taken from the updated *Hipparcos* catalogue (van Leeuwen 2007) and is consistent with SDSS 0832 to within the astrometric uncertainties. Figure 6 shows the proper motion of SDSS 0832 and η Cancri (as well as SDSS 0838 and SDSS 1638). Figure 7 shows a UKIDSS *JHK* false colour image of SDSS 0832 and η Cancri.

We also obtained all available proper motions from the literature (VizieR/CDS database) for comparison (summarise in Table 3), and note just one minor inconsistency. The literature proper motion of the companion (SDSS J163814.32+321133.5) to SDSS 1638 ($\mu_{RA} = -61\pm10$, $\mu_{Dec} = 9\pm10$) was seen to be somewhat smaller than our initial database-measured proper motion ($\mu_{RA} = -85\pm10$, $\mu_{Dec} = 2\pm10$). We therefore re-measured the proper motion of

SDSS J163814.32+321133.5 and SDSS 1638 using a careful selection of fiducial reference stars and the IRAF routines GEOMAP and GEOXYTRAN. The results ($\mu_{RA} = -68\pm15$, $\mu_{Dec} = -4\pm12$ for SDSS J163814.32+321133.5; $\mu_{RA} = -82\pm15$, $\mu_{Dec} = 9\pm12$ for SDSS 1638) show a good agreement with literature values, and we conclude that in this case the proper motion measured direct from the database coordinate/epoch information was not optimal.

Overall, we thus found nine star + ultra-cool dwarf common proper motion pairs. Proper motions of seven of these are shown in Figure 8, and the proper motions of the other two (SDSS 0832 and SDSS 1638) are shown in Figure 6 for clarity. Table 4 shows the parameters of the eight dwarf star + ultra-cool dwarfs common proper motion pairs, and Fig-

Table 4. Parameters of eight ultra-cool dwarf binary systems.

Binary Component	A TYC 1189-1216-1	B SDSS 0101	A G 3-40	B SDSS 0207	A LP 312-49	B SDSS 0858	A LP 548-50	B SDSS 0953
Sp. Type	K5	M9.5^g	M1.5	L3^c	M4	L0^d	M4	M9.5^g
SDSS RA	01 01 55.00	01 01 53.11	02 07 37.47	02 07 35.59	08 58 36.75	08 58 36.97	09 53 24.20	09 53 24.54
SDSS Dec	15 28 01.2	15 28 19.4	13 54 49.4	13 55 56.2	27 11 05.8	27 10 50.8	05 27 00.9	05 26 58.4
Dist (pc)	55±15	60±18	35^e±8	37±10	52±10	46±11	62±10	65±13
Dist.b^a(pc)	...	85±18	...	53±10	...	65±11	...	92±13
$\mu_{\rm RA}$(mas/yr)	20±2	27±17	262±2	272±14	88±6	104±17	−186±3	−203±22
$\mu_{\rm Dec}$(mas/yr)	37±2	43±14	−179±2	−173±13	−199±3	−184±17	38±3	47±16
V	11.49±0.15	...	12.50±0.13	...	16.19	...	17.96	...
SDSS i	12.79±0.01	19.57±0.03	11.01±0.01	19.75±0.03	14.34±0.01	19.44±0.02	15.64±0.01	19.70±0.04
SDSS z	10.95±0.01	17.74±0.02	11.24±0.01	17.99±0.02	13.49±0.01	17.64±0.02	14.69±0.01	17.83±0.03
UKIDSS Y	...^{f}	16.31±0.01	...^{f}	16.59±0.01	...	...	...	...
UKIDSS J	...^{f}	15.31±0.01	...^{f}	15.37±0.01	11.92±0.01	15.01±0.01	13.12±0.01	...
UKIDSS H	...^{f}	14.68±0.01	...^{f}	14.53±0.01	...	...	12.58±0.01	15.05±0.01
UKIDSS K	...^{f}	14.15±0.01	...^{f}	13.83±0.01	...	...	12.24±0.01	14.47±0.01
2MASS J	9.10±0.02	15.49±0.05	9.20±0.02	15.46±0.05	11.99±0.02	15.05±0.05	13.18±0.03	15.67±0.09
2MASS H	8.48±0.03	14.70±0.06	8.57±0.06	14.47±0.04	11.41±0.02	14.23±0.05	12.57±0.03	14.96±0.07
2MASS K	8.34±0.02	14.21±0.06	8.31±0.02	13.81±0.05	11.11±0.02	13.66±0.05	12.29±0.03	14.39±0.08
Separation	36″.6		72″.5		15″.4		5″.7	
Sep. (AU)	2050±571		2538±580		801±154		352±57	
SP^b	4.82×10^{-3}		1.75×10^{-3}		6.60×10^{-5}		1.62×10^{-5}	

Binary Component	A LP 609-3	B SDSS 0956	A SDSS 130432^h	B SDSS 130433^h	A SDSS 163126.17^h	B SDSS 163126.15^h	A SDSS 163814^h	B SDSS 163817^h
Sp. Type	M2	M9^d	M4.5	L0	M5.5	M8^d	M4	L0^d
SDSS RA	09 56 14.86	09 56 13.13	13 04 32.93	13 04 33.16	16 31 26.17	16 31 26.15	16 38 14.32	16 38 17.31
SDSS Dec	01 44 58.7	01 45 14.3	09 07 13.7	09 07 06.9	29 48 47.1	29 48 36.9	32 11 33.5	32 11 44.1
Dist (pc)	98±10	91±28	50±11	51±14	74±32	75±20	51±13	54±14
Dist.b^a(pc)	...	128±28	...	72±14	...	106±20	...	76±14
$\mu_{\rm RA}$(mas/yr)	−104±14	−113±35	−125±3	−102±19	−52±3	−48±11	−66± 6	−82±15
$\mu_{\rm Dec}$(mas/yr)	−189±19	−189±35	18±4	14±19	2±4	5±11	6± 3	9±12
V	15.99	...	16.63±0.34	...	...	...	14.89	...
SDSS i	14.12±0.01	20.30±0.04	14.45±0.01	19.11±0.02	17.07±0.01	18.87±0.01	13.39±0.01	19.81±0.03
SDSS z	13.50±0.01	18.51±0.04	13.52±0.01	17.33±0.02	15.86±0.01	17.34±0.02	12.37±0.01	17.92±0.02
UKIDSS Y	12.62±0.01	17.20±0.02	12.50±0.01	16.32±0.01	...	...	...	...
UKIDSS J	12.12±0.01	16.36±0.01	11.91±0.01	15.28±0.01	14.08±0.01	15.39±0.01	11.00±0.01	15.35±0.01
UKIDSS H	11.66±0.01	15.92±0.01	11.41±0.01	14.59±0.01	...	...	...	...
UKIDSS K	11.40±0.01	15.48±0.02	11.10±0.01	14.03±0.01	...	...	...	...
2MASS J	12.20±0.02	16.24±0.10	11.96±0.02	15.29±0.06	14.15±0.03	15.53±0.06	10.98±0.02	15.39±0.05
2MASS H	11.63±0.03	15.77±0.14	11.38±0.03	14.57±0.07	13.56±0.04	14.85±0.07	10.41±0.02	14.64±0.05
2MASS K	11.40±0.02	15.28±0.19	11.10±0.03	13.95±0.07	13.21±0.04	14.59±0.08	10.16±0.02	14.16±0.07
Separation	30″.4		7″.6		10″.1		46″.0	
Sep. (AU)	2979±304		374±76		756±200		2418±664	
SP^b	3.49×10^{-3}		2.23×10^{-4}		6.57×10^{-4}		8.75×10^{-4}	

^{a} Distances calculation assumes unresolved equal-mass binaries.

^{b} Statistical probability (SP) that the common proper motion could occur by random chance, see section 5.3 for detail of the method.

^{c} Characterized by Hawley et al. (2002) as an L3 dwarf.

^{d} Catalogued by West et al. (2008) as L0, L0, M9 and M8 dwarf.

^{e} The distance given by Lépine & Shara (2005) is 32.5±6.8.

^{f} The star is too bright for UKIDSS, thus JHK magnitudes are not reliable.

^{g} Based on optical – near-infrared colours.

^{h} We used more digital number in their name to distinguish the two components, SDSS 1304, SDSS 1631, SDSS 1638 will reference to secondary ultra-cool dwarfs in this paper.
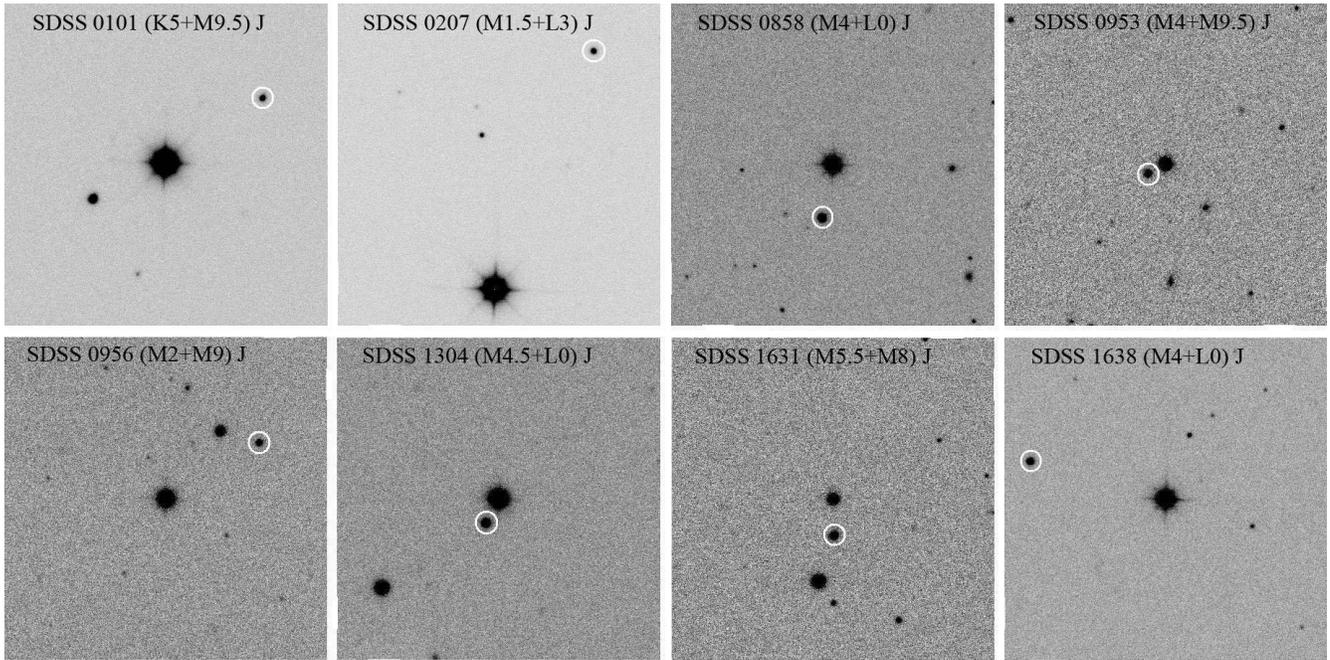
Figure 9. UKIDSS J-band images of eight ultra-cool dwarf binary systems. All the images have a size of 1.5 arcmin with north up and east left. The primary stars are generally in the centre of imges, except the second one (SDSS 0207) in which the primary star is in the bottom of the field, the ultra-cool dwarfs are in *white circles*.

ure 9 shows UKIDSS $J-$band images of these systems. The η Cancri system is discussed further in Section 6.

5.4   Chance alignments?

To determine if the new binary systems are genuine, we carried out a statistical analysis of the probability that the pairs could be line-of-sight associations with photometry and proper motion consistent with binarity by random chance (using a similar method to that used by Day-Jones et al. (2008)). As an example we discuss the case of η Cancri and SDSS 0832. To assess the probability of common proper motion we searched the SuperCOSMOS Science Archive (Hambly et al. 2001) in a square degree of sky around the position of the L dwarf, and made a colour-magnitude selection (B versus B−R) consistent with a dwarf sequence in the ∼90-160 pc distance range. We found that seven out of 337 objects had common proper motion to within 2 sigma uncertainty, suggesting a probability of 2 per cent that such common proper motion could occur by random chance. Separations out to 164″ from η Cancri and a distance range of 90−160 pc correspond to a space volume of 2.86 pc^3. Assuming a space density of 0.0106 pc^{-3} for ∼G-K stars (M_V=5.5-8.5; Kroupa 1995), we thus estimate that we would expect 4.9×10^{-4} G or K stars to masquerade as common proper motion companions in the volume considered around the L dwarf SDSS 0832.

Our full ultra-cool dwarf sample contains 268 objects with proper motion $>$ 100 mas/yr, 283 with proper motion = 50-100 mas/yr, and 258 with proper motion $<$ 50 mas/yr. η Cancri resides in our lowest proper motion group, and companions to ultra-cool dwarfs in this group were searched for (in all but 2 cases) out to separations of 2′. Accounting for the typical volume searched around each ultra-cool dwarf,

and the total number of ultra-cool dwarfs in this group, we estimate that we might have expected to find ∼0.05 apparent η Cancri-like common proper motion companions by random chance. We performed similar calculations for our other binary systems, using a K-M space density of 0.04 pc^{-3} (Kroupa 1995) and accounting for the significantly smaller separations and generally larger proper motions (see Table 4). We note that the expected number of random chance alignments for these other systems (0.00002−0.0048) are much less than for the η Cancri system. This analysis shows that overall we would not expect any random chance common proper motion companions to our full ultra-cool dwarf sample, and that our nine identified systems should be genuine binaries. However, we note that for the wide separation and lower proper motion of η Cancri B, the possibility of spurious companionship is larger (although still very small) than for the other binaries.

5.5   New binaries

Figure 10 shows the distance constraints of the nine binary ultra-cool dwarfs plotted against the distance constraints for their respective primary stars. Distances of the seven brighter primary dwarfs are based on the relationship between the $V-J$ colour index and absolute magnitude M_V (Lépine 2005). However, SDSS J163126.17+294847.1 (M5.5V) is too faint and red to have a V-band magnitude available, so we constrained its distance using the same method that was used for the ultra-cool dwarfs (see Section 4). The distance of η Cancri is from *Hipparcos* (van Leeuwen 2007). This plot allows us to place constraints on possible unresolved binarity amongst our ultra-cool dwarf companions. It can be seen that six ultra-cool dwarfs could be equal-mass unresolved binaries by the distance constraints. We

Table 2. Proper motions and distance estimates for the 34 new L dwarfs.

Name	μ_{RA}[a] (mas/yr)	μ_{Dec}[a] (mas/yr)	Distance[b] (pc)	Sp.T.
SDSS 0006	-5 ± 19	-40 ± 19	94 ± 29	L0
SDSS 0040	121 ± 37	-62 ± 37	111 ± 39	L0
SDSS 0843	150 ± 10	-574 ± 10	32 ± 9	L2
SDSS 0844	40 ± 7	-98 ± 7	51 ± 15	L2
SDSS 0846	19 ± 19	-18 ± 19	69 ± 21	L0
SDSS 0921	-136 ± 15	-81 ± 15	57 ± 17	L1
SDSS 093215	40 ± 25	-74 ± 25	77 ± 15	L2
SDSS 093242	23 ± 11	12 ± 11	61 ± 18	L0
SDSS 0936	-49 ± 13	-38 ± 13	51 ± 15	L3
SDSS 0938	-12 ± 11	-38 ± 11	50 ± 15	L0
SDSS 0941	-63 ± 46	-362 ± 46	102 ± 32	L0
SDSS 1013	17 ± 32	28 ± 32	79 ± 25	L0
SDSS 1213	-292 ± 30	-186 ± 30	49 ± 8	L4
SDSS 1219	-32 ± 30	-13 ± 30	62 ± 18	L0
SDSS 1245	4 ± 18	-43 ± 18	64 ± 19	L1
SDSS 1252	-66 ± 23	-50 ± 23	48 ± 14	L3
SDSS 1253	-14 ± 21	-1 ± 21	78 ± 24	L0
SDSS 1304	-102 ± 19	14 ± 19	51 ± 14	L0
SDSS 1308	-234 ± 13	45 ± 13	48 ± 14	L0
SDSS 1327	-162 ± 22	29 ± 22	33 ± 9	L1
SDSS 1346	-221 ± 19	-93 ± 19	43 ± 13	L3
SDSS 1422	-159 ± 11	-571 ± 11	32 ± 9	L3
SDSS 1439	-130 ± 19	-3 ± 19	47 ± 14	L1
SDSS 1440	-26 ± 26	10 ± 26	43 ± 7	L4
SDSS 1452	65 ± 19	-191 ± 19	55 ± 16	L0
SDSS 1456	37 ± 17	-16 ± 17	48 ± 7	L4
SDSS 1503	22 ± 36	96 ± 36	63 ± 19	L2
SDSS 1523	0.4 ± 19	-19 ± 19	74 ± 22	L0
SDSS 1623	-265 ± 16	-1 ± 16	43 ± 7	L4
SDSS 1637	-226 ± 13	-86 ± 13	44 ± 13	L0
SDSS 1649	-27 ± 21	15 ± 21	66 ± 20	L1
SDSS 2205	51 ± 33	75 ± 33	104 ± 27	L0
SDSS 2336	-44 ± 45	-27 ± 45	117 ± 31	L0
SDSS 2347	13 ± 40	-6 ± 40	86 ± 23	L0

[a] 2MASS-UKIDSS data-base proper motions − found by dividing the difference between the 2MASS and SDSS coordinates (from the respective databases) by the observational epoch difference. Standard errors are calculated using the major axes of the position error ellipses from 2MASS and SDSS. [b] Distance are based on M_J−spectral type relationship (Hawley et al. 2002).

can't, however, rule out the possibility of non-equal-mass unresolved binarity from this plot. If SDSS 0832 for example was an equal-mass binary, it would be too distant to be associated with η Cancri. However, a non-equal-mass binary (e.g. an unresolved L + T binary) would affect spectral type and distance estimates as well as absolute magnitude, and this is not ruled out by Figure 10. This will be discussed further in Section 6.3.

Figure 11 shows our new ultra-cool dwarf + star binaries in the context of the broader population of such wide systems (we plot known binaries with a>100AU; see Faherty et al. 2010; Artigau et al. 2009; Burningham et al. 2009; Radigan et al. 2009, 2008; Phan-Bao et al. 2008; Caballero et al. 2007; Cruz et al. 2007; Luhman et al. 2007; Mugrauer et al. 2007; Metchev et al. 2006; Reid et al. 2006; Billères et al. 2005; Chauvin et al. 2005; Neuhäuser et al. 2005, 2004; Seifahrt et al. 2005a,b; Golimowski et al. 2004; Scholz et al. 2004, 2003; Bouy et al. 2003; Gizis et al. 2001, 2000; Wil-

Table 5. Parameters of SDSS 0838: a candidate Praesepe member.

| Parameter		Value
RA (J2000)	....	08 38 23.69
Dec (J2000)	....	16 47 02.0
Sp. Type	....	L0.5
Dist[a] (pc)	....	181 ± 62
Dist.b[a] (pc)	....	256 ± 62
μ_{RA} (mas/yr)	....	-21 ± 15
μ_{Dec} (mas/yr)	....	-19 ± 15
SDSS r	....	24.28 ± 0.53
SDSS i	....	22.32 ± 0.21
SDSS z	....	20.41 ± 0.18
UKIDSS Y	....	19.24 ± 0.08
UKIDSS J	....	18.29 ± 0.06
UKIDSS H	....	17.74 ± 0.07
UKIDSS K	....	17.02 ± 0.06
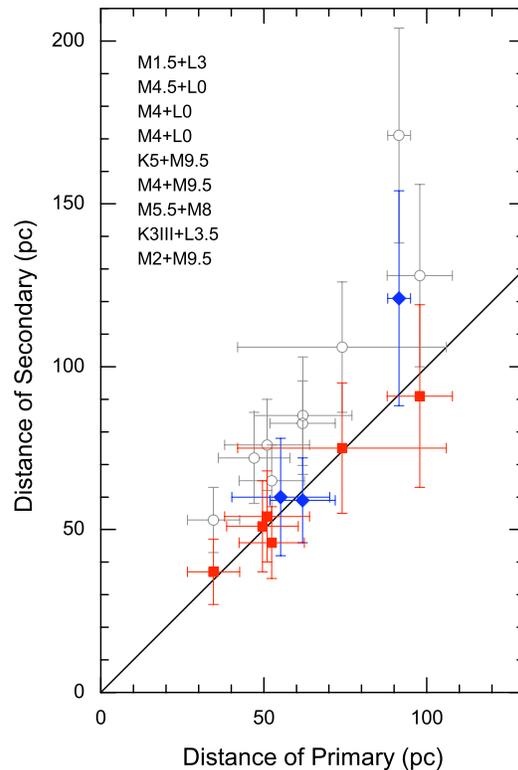
Figure 10. Distances of ultra-cool dwarfs (from left to right: SDSS 0207, 1304, 1638, 0858, 0953, 0101, 1631, 0832, 0956) and their primary stars. Spectral types of combinations are listed in according distance of primaries in the top left of the plot. The *red squares* and *blue diamonds* indicate the objects with and without SDSS spectra respectively. The *gray open circles* show the distances of ultra-cool dwarfs assume as unresolved equal-mass binaries.

Table 6. Parameters of η Cancri AB.

Parameter	Adopted Value	Reference/Note
Separation (AU)	15019^{+562}_{-522} $(164''.16)$	This paper
Distance (pc)	$91.5^{+3.5}_{-3.2}$	van Leeuwen (2007)
SP	0.05	This paper
η Cancri A		
Sp. Type	K3III	Perryman (1997)
RA (J2000)	08 32 42.50	SDSS (2004)
Dec (J2000)	20 26 27.7	SDSS (2004)
V	5.330 ± 0.004	Kharchenko (2000)
$B-V$	1.252 ± 0.002	Perryman (1997)
$V-I$	1.11 ± 0.04	Perryman (1997)
J	3.49 ± 0.30	2MASS
H	2.86 ± 0.21	2MASS
K	2.70 ± 0.32	2MASS
Parallax (mas)	10.93 ± 0.40	van Leeuwen (2007)
$\mu_{\rm RA}$ (mas/yr)	-46.33 ± 0.43	van Leeuwen (2007)
$\mu_{\rm Dec}$ (mas/yr)	-44.31 ± 0.24	van Leeuwen (2007)
U (km/s)	-27.1	Famaey (2005)
V (km/s)	-24.6	Famaey (2005)
W (km/s)	-10.7	Famaey (2005)
$T_{\rm eff}$ (K)	$4446^a\pm80$	Luck (2007) Hekker (2007) Allende Prieto (1999)
log $(L/L_\odot)$	1.95 ± 0.06	Luck (2007)
Mass $(M_\odot)$	$1.4^b\pm0.2$	Luck (2007) Allende Prieto (1999)
Radius $(R_\odot)$	$16.0^{c+1.8}_{-1.6}$	This paper
g (cm/s^2)	2.24 ± 0.09 dex	Luck (2007)
[Fe/H]	$0.0^d\pm0.1$	This paper
Age (Gyr)	$2.2-6.1$	This paper
η Cancri B (SDSS 0832)		
Sp. Type	L3.5$\pm1.5^e$	This paper
RA (J2000)	08 32 31.87	SDSS (2004)
Dec (J2000)	20 27 00.0	SDSS (2004)
Dist (pc)	121 ± 33	This paper
Dist.b (pc)	171 ± 33	This paper
$\mu_{\rm RA}$ (mas/yr)	-47.4 ± 8.2	This paper
$\mu_{\rm Dec}$ (mas/yr)	-38.9 ± 8.2	This paper
r	25.37 ± 0.63	SDSS
i	22.13 ± 0.17	SDSS
z	20.15 ± 0.12	SDSS
Z	19.69 ± 0.09	UKIDSS
Y	18.66 ± 0.05	UKIDSS
J	17.74 ± 0.04	UKIDSS
H	17.16 ± 0.04	UKIDSS
K	16.52 ± 0.04	UKIDSS
Mass (M_{Jup})	$63-82$	e
$T_{\rm eff}$ (K)	1800 ± 150	e
g (cm/s^2)	$5.3-5.5$ dex	e

^{a} This is the average $T_{\rm eff}$ of Luck (2007), Hekker (2007) and Allende Prieto (1999). ^{b} This is average mass of Luck (2007) and Allende Prieto (1999). ^{c} Based on log $(L/L_\odot)$ (Luck & Heiter 2007) and $T_{\rm eff}$ (4446 K). Note that the radius given in Allende Prieto et al. (1999) is $17.0^{+2.5}_{-2.2}$ R$_\odot$ along with a lower $T_{\rm eff}$ (4365 K). ^{d} This is medium value of Luck (2007), Hekker (2007) and Brown (1989). ^{e} Based on Lyon duty model (Chabrier et al. 2000) and Burrows et al. (2006, 1997) model, assume as a single object at the same distance with η Cancri A.
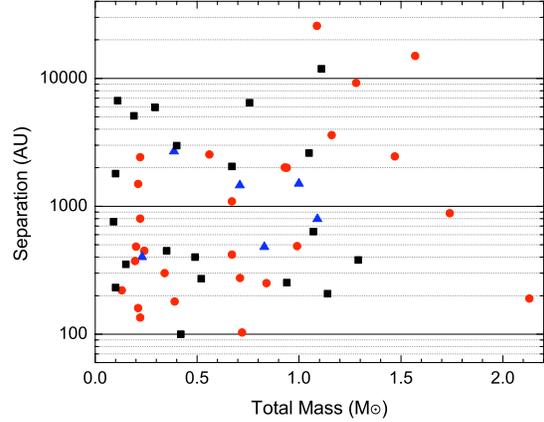
Figure 11. Total mass versus separation for binaries have projected separation larger 100 AU. *Black squares*, *red circles* and *blue triangles* are binaries with late M, L and T secondaries.

son et al. 2001; Burgasser et al. 2000; Lowrance et al. 2000; White et al. 1999; Rebolo et al. 1998). It is clear from this plot that the projected separation range <7000AU is well populated for binaries with a total mass <1M$_\odot$, with wider ultra-cool dwarf companions to such stars being rare. However, there is some indication that higher mass primaries are able to host wider ultra-cool dwarf companions, with the η Cancri system contributing to this trend.

6 ETA CANCRI AB

With a separation of 15019 AU, η Cancri AB is an extremely wide binary, however, as Section 5.4 explains, it is a statistically solid association, with the two components presumably having a common composition and age. Only five brown dwarf mass objects were previously known around (four) giant stars, all detected by the radial velocity method (Hatzes et al. 2005; Lovis & Mayor 2007; Liu et al. 2008b; Niedzielski et al. 2009). These objects all have $m \sin i$ in the range $10-20$ M$_{Jup}$ and are within three AU of their primaries. They are thus unobservable with current technology, and their mass range overlaps that of the planetary regime. As such, their atmospheres may not share the same composition as the primary star, and without direct observation they are not useful benchmark objects for study.

6.1 The metallicity of η Cancri A

η Cancri A is a bright K3 giant with a V band magnitude of 5.33, and it's metallicity has been measured several times by various groups; [Fe/H] = 0.19 by Brown et al. (1989), [Fe/H]=0.07±0.21, [Fe/H] = 0.08, [Fe I/H] = 0.02, [Fe II/H] = 0.10 measured with different methods by Luck & Heiter (2007) and A(Fe) = 7.64 by Hekker & Meléndez (2007). These results are consistent with a metallicity of [Fe/H]=0.10±0.1 for η Cancri A. Given the importance of being able to infer a metallicity for the L dwarf companion,
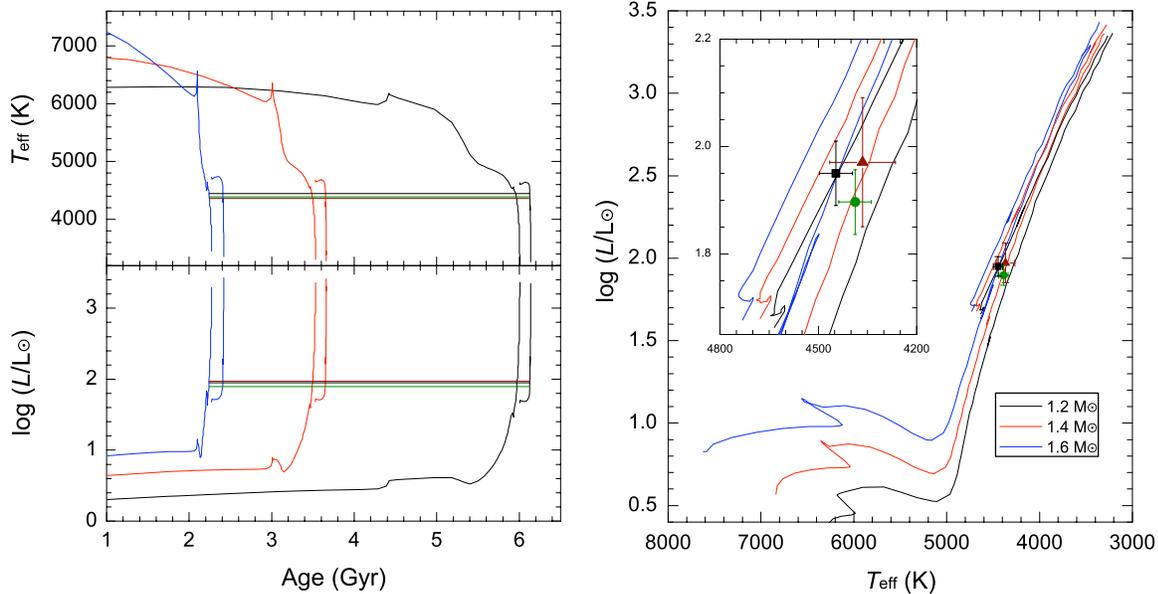
Figure 12. $T_{\rm eff}$ and L evolutionary tracks (Girardi et al. 2000) of solar metallicity stars with different masses (1.2M$_\odot$, *black lines*; 1.4M$_\odot$, *red lines*; 1.6M$_\odot$, *blue lines*). The *filled black square* (4446, 1.95) in the right panel represents the average $T_{\rm eff}$ from the literature and L from Luck & Heiter (2007). The *filled green circle* (4388, 1.90) represents the values from PARAM (da Silva et al. 2006). The *filled brown triangle* (4365, 1.97) represents the values from Allende Prieto et al. (1999). *Horizontal lines* in left hand plots indicated these L and $T_{\rm eff}$ values in the same colours with symbols in right hand plots.

we have re-addressed the metallicity of this system with new data and analysis.

We obtained a high resolution echelle spectrum of η Cancri A during an observing run from 9 to 11 February 2009, using the FIber fed Echelle Spectrograph (FIES) at the 2.56 m Nordic Optical Telescope located at the Observatorio del Roque de los Muchachos (La Palma, Spain). We used FIES with a 2048×2048 13.5μm pixel EEV42-40 CCD detector. The wavelength range covered is from 3620 to 7360 Å in 80 orders. The reciprocal dispersion ranges from 0.02 to 0.04 Å/pixel and the spectral resolution (FWHM) is from 0.06 to 0.10 Å. We extracted the spectrum using standard reduction procedures in IRAF, including bias subtraction, flat-field division and optimal extraction of the spectra. We obtained the wavelength calibration by taking a spectrum of a Th-Ar lamp. Finally, we normalized the spectrum by a polynomial fit to the observed continuum.

Stellar iron abundances $[A(\rm Fe) = \log N(\rm Fe)/N(\rm H) + 12]$ were estimated from the equivalent width measurements of a set of thirteen Fe I and two Fe II lines. The line list was provided by Jorge Meléndez (private communication) who has tested their use for F, G and K giant stars. Measurements were compared with equivalent widths computed under the assumption of local thermodynamical equilibrium (LTE) and spherical symmetry, which for stars of low surface gravity should be more appropriate than a plane-parallel description. Calculations were made using the Uppsala suite of codes and the new MARCS model atmospheres (Gustafsson

et al. 2008). Stellar atmospheres are characterised by four fundamental parameters: $T_{\rm eff}$, $\log g$, metallicity ([Fe/H] = $A(\rm Fe) - A(\rm Fe)_\odot$) and microturbulence ($\xi_t$). For the values of interest here, a grid of model atmospheres of one solar mass and standard composition was linearly interpolated. The $T_{\rm eff}$ of η Cancri A was estimated from Johnson photometry in the blue ($V = 5.343$ and $B = 6.608$) and 2MASS in the red ($J = 3.489$, $H = 2.861$ and $K = 2.699$), using the Ramírez et al. (2005) $T_{\rm eff}$-vs-$(B - V)$, $(V - H)$, $(V - J)$ and $(V - K)$ calibrations. Estimates coming from the blue and the red were somewhat different, 4329 K versus 4520 K, so an average value of 4472 K with an assigned 107 K uncertainty in our computations. The interstellar extinction of this nearby star estimated from the models in Hakkila et al. (1997) is very low $E(B - V) = 0.01 \pm 0.05$ and it cannot explain the temperature discrepancy between these two estimates. Also we tried the new $T_{\rm eff}$-vs-colour calibrations in González Hernández et al. (2009) but the difference is even larger ($T_{\rm eff}$ 4531 $\pm$ 137) with the blue estimate. Another concern is the precision of the surface gravity determination which in turns compromises the accuracy of the metallicity determinations. Our $\log g = 2.30$ estimate is based on the Hipparcos parallax of the star ($\pi = 10.93 \pm 0.43$, van Leeuwen 2007), and on a $M \sim 1.60$ $M_\odot$ stellar mass and a $BC = -0.558$ bolometric correction for V. These two last values are estimated from isochrones and were taken from Luck & Heiter (2007) after checking they were appropriate for our stellar temperature and metallicity values (for
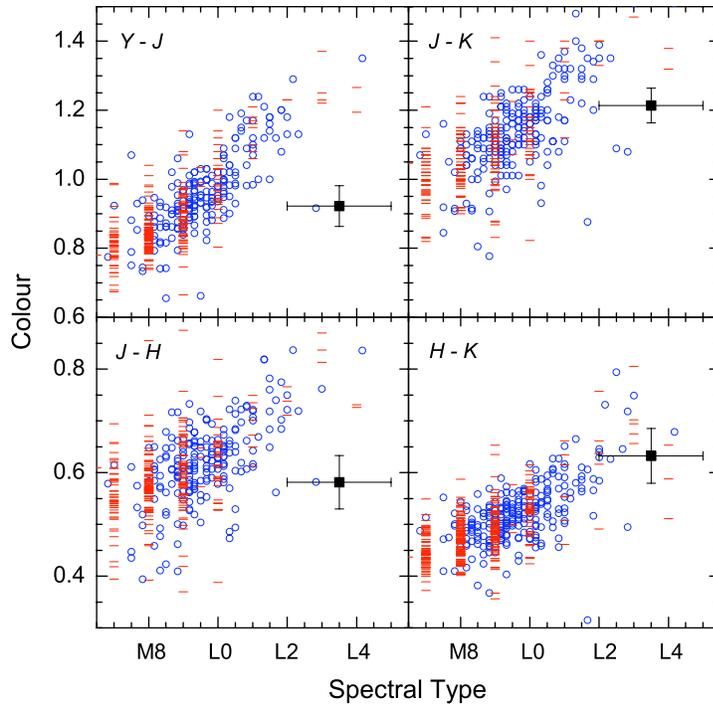
Figure 13. UKIDSS *YJHK* colours of η Cancri B (*black squares*) and ultra-cool dwarfs with (*red bars*) and without (*blue circles*) spectra, as a function of spectral type.

details on the accuracy of these parameter determinations see Luck & Heiter (2007)). Another way of estimating the surface gravity is the Fe ionization equilibrium, however, this method has the disavantage of being sensitive to departures from LTE. In our case, our best estimate of $\log g$ (2.30) produces an abundance difference between Fe I and Fe II of $\Delta A(\text{Fe}) = 0.15$ dex. The microturbulence value was changed until the trend in $A(\text{Fe})$-vs-FeI equivalent widths was minimised, which happened at $\xi_t = 1.62$ km/s.

The method employed here requires the knowledge a priori of the metallicity so that two iterations were necessary to get our best iron abundance value of 7.52 dex (an average value over the fifteen Fe lines). Results based on the Fe II lines are sensitive to the uncertainties of the stellar parameters: abundance changes of -0.12 dex for $\Delta T_{\text{eff}} \sim 100$ K, 0.08 dex for $\Delta \log g \sim 0.15$ (mass, parallax), 0.05 dex for $\Delta[\text{Fe/H}] \sim 0.10$ dex. However, the average abundance based on the neutral lines is much less sensitive (abundance changes ~ 0.02-0.03 dex). Changes in the microturbulence and the uncertainties in the measured equivalent widths have a more significant effect, 0.05 dex for 0.1 km/s microturbulence changes, and a similar effect for a typical $\Delta W_\lambda = 3$ mÅ uncertainty. We have adopted our total error budget to be ± 0.10 dex, the standard deviation associated with the fifteen lines used, which will partially account for the sensitivity mentioned before. We also note that our abundances may suffer from other systemactic errors, e.g. T_{eff} zero points, isochrones uncertainties, departures from LTE. Our final metallicity value depends on the solar iron

abundance that we assume; if the Sun was analysed in a similar way to η Cancri A (i.e. 1D-LTE but using the appropriate line list e.g. García Pérez et al. 2006), then the metallicity (relative to solar) of η Cancri A would be -0.02 dex [$A(\text{Fe})_\odot = 7.54$]. Solar abundances based on 3D-LTE analysis are much lower, 7.45 Grevesse et al. (2007), which leads to higher metallicity value for η Cancri A of 0.07 dex. On balance we present a metallicity constraint (in Table 6) for η Cancri A of 0.0±0.1.

6.2   The age of η Cancri A

The T_{eff} measurements of η Cancri A measured here and by Allende Prieto et al. (1999); Luck & Heiter (2007); Hekker & Meléndez (2007) are all consistent with $T_{\text{eff}} = 4450 \pm 100$ K. The radius of η Cancri A based on this temperature and $\log (L/L_\odot) = 1.95 \pm 0.06$ (Luck & Heiter 2007) is $16.0^{+1.8}_{-1.6}$ $R_\odot$. Luck & Heiter (2007) estimated a mass for η Cancri A of 1.6 ± 0.5 $M_\odot$ (typical uncertainty $\sim 35\%$), and Allende Prieto et al. (1999) estimates a mass of 1.36 ± 0.67 $M_\odot$. To provide additional refinement, we calculated the parameters of η Cancri A with PARAM (da Silva et al. 2006). PARAM is a web interface for the Bayesian estimation of stellar parameters. Table 7 shows our input and output values from PARAM. The [Fe/H], V magnitude, parallax, and $B - V$ colour of η Cancri A are known, so we experimented with different T_{eff} input values until the model colour output was $B - V = 1.252$ (Perryman et al. 1997). The mass, gravity and radius output from PARAM are all consistent with
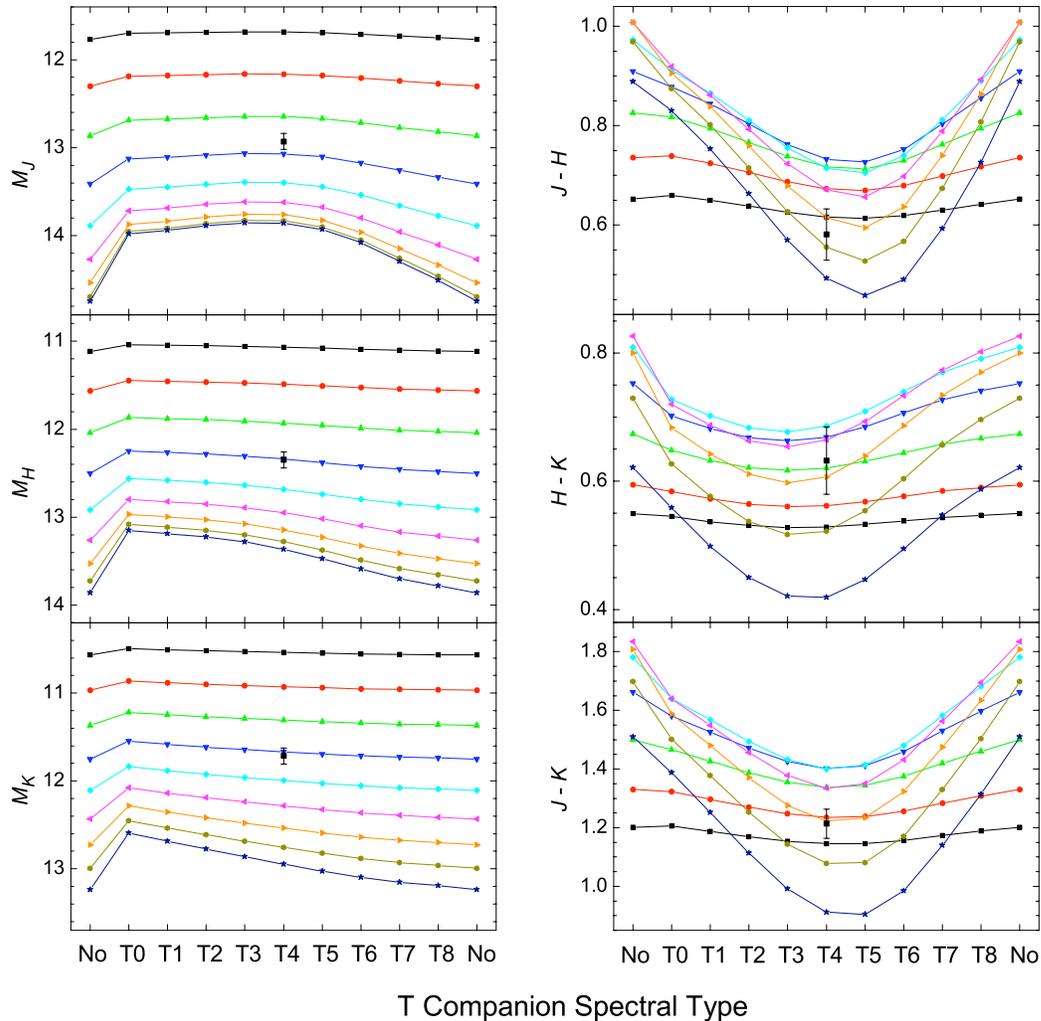
Figure 14. *JHK* absolute magnitudes and colours of unresolved L+T binaries. Different *lines* represent absolute magnitudes and colours of L dwarf primaries (L1−L9, from top to bottom in left panel) without or with different T companions (T0−T8). If η Cancri B (*black square*) is actually an unresolved binary, then the constituents would likely be made up of an L4 and a T4 dwarf.

other estimates, but provide a somewhat improved level of accuracy, and on balance we assumed a mass of 1.40±0.2 M$_\odot$ for η Cancri A.

We have used these physical properties to constrain the age of η Cancri A by comparison to evolutionary tracks. Figure 12 shows the $T_{\rm eff}$ and L evolutionary tracks (Girardi et al. 2000) as a function of time and on a Hertzsprung−Russell (HR) diagram for solar metallicity stars with different masses (1.2M$_\odot$, 1.4M$_\odot$, and 1.6M$_\odot$). $T_{\rm eff}$ and log $(L/L_\odot)$ measurements from the literature are plotted in the HR diagram with different symbols (see caption). In the left-hand plots we indicate with open symbols where the measured values of luminosity and $T_{\rm eff}$ intersect with the evolutionary model tracks. In this way the (Girardi et al. 2000) evolutionary models lead to an age constraint of 2.2−6.1 Gyrs.

We have also used the Hurley et al. (2000) stellar evo-

Table 7. Input and output values from PARAM for η Cancri.

	Input value		Output value
$T_{\rm eff}$	4388^a±80 K	Age	3.61±1.86 Gyr
$[{\rm Fe/H}]^b$	0.025±0.100	Mass	1.36±0.23 M$_\odot$
V^b	5.330±0.004	g	2.16±0.11 dex (cm/s^2)
Parallax^b	10.93±0.40mas	R	15.4±1.1 R$_\odot$
		$B-V$	1.252^c±0.038

Note: PARAM is a web interface for the Bayesian estimation of stellar parameters, http://stev.oapd.inaf.it/cgi-bin/param (da Silva et al. 2006).

[a] This is an estimated value to get the right $B-V$ value.

[b] Values are from literatures.

[c] This value equal to observed value.

lution sequence with initial masses $1.2-1.6$ M$_\odot$ (ΔM = 0.05 M$_\odot$) and metallicity [Fe/H] = 0.0 and 0.10. Using the same approach as in Figure 12, these models give an age range of $2.4-6.6$ Gyr for η Cancri A which is very similar to the result from the Girardi et al. (2000) model. In addition we note that the age estimate from PARAM is also consistent with these values estimated directly from evolutionary tracks. A summary of the properties of η Cancri A is given in Table 6.

6.3 The properties of η Cancri B

As a single ultra-cool dwarf: We can assume that the distance of η Cancri B is essentially the same as that of η Cancri A. Although since this is a very wide binary system we have increased the uncertainty of the companion distance slightly to account for η Cancri B potentially being $\sim$ 0.5 pc closer or further than the primary along the line of sight. This allows us to place resonably tight constraints on the absolute brightness of this ultra-cool dwarf. η Cancri B must have $M_J = 12.93\pm0.09$, $M_H = 12.35\pm0.09$ and $M_K = 11.72\pm0.09$. Using the $M_{JHK}-$ spectral type relations of Liu et al. (2006) we thus estimate that its spectral type must be L3-4 if it is a single L dwarf. Combining these magnitudes and an age (inferred from η Cancri A), the evolutionary model of Chabrier et al. (2000) predicts that mass = $63-74$ M$_{Jup}$, $T_{\rm eff} = 1805\pm115$ K and log $(g/{\rm cms}^{-2}) = 5.31-5.36$. Using an alternative model set (Burrows et al. 2006) yields a slightly higher mass or $75-82$M$_{Jup}$, and corresponding $T_{\rm eff} =1800\pm150$ K, log $(g/{\rm cms}^{-2}) = 5.38-5.48$.

In Figure 13 we compare the colour of η Cancri B to our large population of SDSS ultra-cool dwarfs, and it can be seen that its colours appear somewhat discrepant from other early L dwarfs. While it has similar H-K to the bulk population, its $J-K$ colour is only similar to the bluer L dwarfs and its $Y-J$ and $J-H$ colours are significantly bluer than typical ultra-cool dwarfs of similar spectral type. Theoretical model colour trends suggest that L dwarfs with low metallicity or higher gravity could have bluer near-infrared colours (Burrows et al. 2006). However, the constraints we have placed on the properties of this benchmark object are not consistent with this interpretation, and the colours of η Cancri B are either at odds with the model trends, or are indicative of unresolved multiplicity.

As an unresolved binary ultra-cool dwarf: We investigated the possibility that the colours of η Cancri B may result from unresolved binarity. T dwarfs have slightly bluer $Y-J$ and significantly bluer $J-H$ and $J-K$ than L dwarfs (Knapp et al. 2004; Pinfield et al. 2008). Combining the light of an L and T dwarf could thus result in these colours being bluer than those of a single L dwarf. We experimented by combining the photometric brightnesses of a variety of L and T dwarf combinations, using the spectral type$-$M$_{JHK}$ polynomial relations from Liu et al. (2006) to provide absolute magnitudes for flux combination. Figure 14 shows the JHK absolute magnitudes and colours of the range of unresolved L-T binaries that we considered. The location of η Cancri B is indicated with it appropriate uncertainties. Considering the full range of colour and magnitude criteria, as well as the intrinsic scatter in the Liu et al. (2006) polynomial fits, we deduce that a combination of an L4 and T4 dwarf at the distance of η Cancri A would have colours and magnitudes

Table 8. Parameters of an L4 and a T4 dwarf from the Lyon group and Burrows group models.

Spectral Type	L4[a]	T4[b]
$M_J{}^c$	13.41±0.37	14.49±0.37
$M_H{}^c$	12.50±0.30	14.46±0.30
$M_K{}^c$	11.75±0.34	14.52±0.34
Mass^d (M$_{Jup}$)	$59-80$	$40-70$
$T_{\rm eff}{}^d$ (K)	1675±145	1140±120
g^d (cm/s^2)	$5.3-5.5$ dex	$5.1-5.4$ dex

[a] Based on dusty model.

[b] Based on dust-free model.

[c] Based on the relationship between spectral types and absolute magnitudes (J- and K-band) of Liu et al. (2006).

[d] These parameters are for an L4 dwarf and a T4 dwarf at age of $2.2-6.1$ Gyrs.

reasonably consistent with those of η Cancri B. In this case, the physical parametres of these two unresolved objects (estimated from the same evolutionary models as before) are given in Table 8.

7 SUMMARY AND FUTURE WORK

We have identified 34 new L dwarfs and nine ultra-cool dwarf + star common PM binary systems (TYC 1189-1216-1 AB, G 3-40 AB, LP 312-49 AB, LP 548-50 AB, LP 609-3 AB, SDSS J130432.93+090713.7 AB, SDSS J163126.17+294847.1 AB and SDSS J163814.32+321133.5 AB, η Cancri AB). Further observations (parallax, activity and rotation rate) of the K-M dwarf primaries in these systems will provide age (e.g. Faherty et al. 2009) and metallicity (e.g. Johnson & Apps 2009) constraints. η Cancri AB is a K3III + early L system with a projected separation of 15019 AU. η Cancri A has a well constrained parallax distance, and we use new observations and the latest theory to estimate an age of $2.2-6.1$ Gyr and a composition near solar for the system. We thus estimate that η Cancri B (as a single object) has mass = $63-82$M$_{Jup}$, $T_{\rm eff} = 1800\pm150$ K, and log $(g/{\rm cms}^{-2}) = 5.3-5.5$, based on a range of evolutionary models.

It is unclear at this stage if η Cancri B is a single L dwarf with unusual colour or an unresolved L+T binary whose components have fairly typical colours when compared to the bulk population. Quality optical$-$infrared spectroscopy would address this issue in more detail, and establish if the binary explanation remains possible. In ddition adaptive optics observations could resolve the pair if their separation is $> 0.05-0.1$ arcsec (e.g. LHS4009; Montagnier et al. 2006) corresponding to a separation $> 5-10$ AU. If the ultra-cool dwarf is shown to be single then this would provide a surprising result when compared to the models. We could also establish $T_{\rm eff}$ and log g more robustly by obtaining full optical to infrared measurements to constrain the bolometric flux and luminosity (e.g. Burningham et al. 2009). If η Cancri B is a closely separated ultra-cool dwarf binary system, it could be possible to derive dynamical masses for the components over a time-scale of several years, and thus improve the benchmark quality of this object still further through more direct constraints on its mass and log g. A more detailed

examination of the spectral morphology and multiplicity of this benchmark ultracool dwarf will in any event provide rigorous tests for solar metallicity dusty ultracool atmosphere models.

REFERENCES

Abazajian K.N. et al., 2009, ApJS, 182, 543
Adelman-McCarthy J.K. et al., 2008, ApJS, 175, 297
Allende Prieto C., Lambert D.L., 1999, A&A, 352, 555
Artigau É., Lafrenière D., Loïc A., Doyon R., 2009, ApJ, 692, 149
Bihain G., Rebolo R., Béjar V.J.S. et al., 2006, A&A, 458, 805
Billères M., Delfosse X., Beuzit J.-L. et al., 2005, A&A, 440, L55
Bouvier J. et al., 2008, A&A, 481, 661
Bouy H., Brandner W., Martín E.L. et al., 2003, AJ, 126, 1526
Brown J.A., Sneden C., Lambert D.L., Dutchover E. J., 1989, ApJS, 71, 293
Burgasser A.J. et al., 2000, ApJ, 531, L57
Burgasser A.J., Kirkpatrick J.D., Lowrance P.J. 2005, AJ, 129, 2849
Burgasser A.J., McElwain M.W., 2006, AJ, 131, 1007
Burgasser A.J. et al., 2010, ApJ, submitted
Burningham B. et al., 2009, MNRAS, 395, 1237
Burrows A. et al., 1997, ApJ, 491, 856
Burrows A., Sudarsky D., Hubeny I., 2006, ApJ, 640, 1063
Buzzoni B. et al., 1984, ESO Messenger, 38, 9
Caballero J.A., 2007, ApJ, 667, 520
Casali M. et al., 2007, A&A, 467, 777
Casewell S.L., Dobbie P.D., Hodgkin S.T. et al., 2007, MNRAS, 378, 1131
Chabrier G., Baraffe I., Allard F., Hauschildt P., 2000, ApJ, 542, 464
Chappelle R.J., Pinfield D.J., Steele I.A. et al., 2005, MNRAS, 361, 1323
Chauvin G. et al., 2005, A&A, 430, 1027
Chiu K., Fan X., Leggett S.K. et al., 2006, AJ, 131, 2722
Clarke J.R.A., Pinfield D.J., Burningham B. et al., 2009, arXiv: 0805.4772
Covey K.R. et al., 2007, AJ, 134, 2398
Cossburn M.R., Hodgkin S.T., Jameson R.F., Pinfield D.J., 1997, MNRAS, 288L, 23
Cruz K.L., Reid I.N., Liebert J. et al., 2003, AJ, 126, 2421
Cruz K.L. et al., 2007, AJ, 133, 439
Cutri R.M. et al., 2003, The IRSA 2MASS All-Sky Catalog of point sources (Pasadena: NASA/IPAC)
Day-Jones A.C. et al., 2008, MNRAS, 388, 838
da Silva L. et al., 2006, A&A, 458, 609
Deacon N.R., Hambly N.C., King R.R., McCaughrean M.J., 2009, MNRAS, 394, 857

Delfosse X. et al., 1997, A&A, 327, 25

De Simone R., Wu X., Tremaine S., 2004, MNRAS, 350, 627

Ducourant C. et al., 2006, A&A, 448, 1235

Dupuy T.J., Liu M.C., Ireland M.J., 2009, ApJ, 699, 168

Epchtein N., de Batz B., Capoani L. et al., 1997, ESO Messeager, 87, 27

Faherty J.K., Burgasser A.J., West A.A. et al., 2010, AJ, 139, 176

Famaey B., Jorissen A., Luri X. et al., 2005, A&A, 430, 165

Fan X. et al., 2000, AJ, 119, 928

García Pérez A.E., Asplund M., Primas F. et al., 2006, A&A, 451, 621

Geballe T.R. et al., 2002, ApJ, 564, 466

Giclas H.L., Burnham R., Thomas N.G., 1971, Lowell proper motion survey Northern Hemisphere. The G numbered stars. 8991 stars fainter than magnitude 8 with motions $> 0''.26$/year.

Girardi L., Bressan A., Bertelli G., Chiosi C., 2000, A&AS, 141, 371

Gizis J.E., Monet D.G., Reid I.N. et al., 2000, MNRAS, 311, 385

Gizis J.E., Kirkpatrick J.D., 2001, AJ, 121, 2185

Golimowski D.A. et al., 2004, AJ, 128, 1733

González Hernández J.I., Bonifacio P., 2009, A&A, 497, 497

Grevesse N., Asplund M., Sauval A.J., 2007, SSR, 130, 105

Gustafsson B., Edvardsson B., Eriksson K., 2008, A&A, 486, 951

Hakkila J., Myers J.M., Stidham B.J. et al., 1997, AJ, 114, 2043

Hambly N.C. et al., 2001, MNRAS, 326, 1279

Hambly N.C. et al., 2008, MNRAS, 384, 637

Hatzes A.P., Guenther E.W., Endl M. et al., 2005, A&A 437, 743

Hawley S.L. et al., 2002, AJ, 123, 3409

Hekker S., Meléndez J., 2007, A&A, 475, 1003

Hewett P.C., Warren S.J., Leggett S.K., Hodgkin S.T., 2006, MNRAS, 367, 454

Hodapp K.W. et al., 2003, PASP, 115, 1388

Hog E. et al., 2000, A&A, 355L, 27

Hogan E., Jameson R.F., Casewell S.L. et al. 2008, MNRAS, 388, 495

Hurley J.R., Pols O.R., Tout C.A., 2000, MNRAS, 315, 543

Ivanov G.A., 2008, KFNT, 24, 480

Jenkins J. et al., 2009, MNRAS, 398, 911

Johnson J.A., Apps K., 2009, ApJ, 699, 933

Kendall T.R., Jones H.R.A., Pinfield D.J. et al., 2007, MNRAS, 374, 445

Kharchenko N.V., 2001, KFNT, 17, 409

Kharchenko N.V., Piskunov A.E., Röser S. et al., 2004, AN, 325, 740

Kirkpatrick J.D. et al., 1999, ApJ, 519, 802

Kirkpatrick J.D. et al., 2000, AJ, 120, 447

Knapp G.R. et al., 2004, AJ, 127, 3553

Kroupa P., 1995, ApJ, 453, 350

Lawrence A. et al., 2007, MNRAS, 379, 1599

Lépine S., Shara M.M., 2005, AJ, 129, 1483

Lépine S., 2005, AJ, 130, 1680

Liu M.C., Leggett S.K., Golimowski D.A. et al., 2006, ApJ, 647, 1393

Liu M.C., Dupuy T.J., Ireland M.J., 2008a, ApJ, 689, 436

Liu Y.-J. et al., 2008b, ApJ, 672, 553

Lovis C., Mayor M., 2007, A&A, 472, 657

Lowrance P.J. et al., 1999, ApJ, 512, L69

Lowrance P.J. et al., 2000, ApJ, 541, 390

Luck R.E., Heiter U., 2007, AJ, 133, 2464

Luhman K.L. et al., 2007, ApJ, 654, 570

Luyten W.J., Hughes H.S., 1980, Proper motion survey with the forty-eight inch Schmidt telescope. LV. First supplement to the NLTT catalogue (Mineapolis, NM: Univ. of Minnesota).

Magazzù A., Martín E.L., Rebolo R., 1993, ApJ, 404, L17

Magazzù A., Rebolo R., Zapatero Osorio M.R. et al., 1998, ApJ, 497, L47

Martín E.L., Rebolo R., Zapatero Osorio, M.R.,1996, ApJ, 469, 706

Martín E.L., Basri G., Zapatero Osorio M.R., Rebolo R., García Lòpez R.J.,1998, ApJ, 507, L41

Metchev S.A., Hillenbrand L.A. 2006, ApJ, 651, 1166

Monet D.G. et al., 2003, AJ, 125, 984

Montagnier G. et al., 2006, A&A, 460, L19

Mugrauer M., Seifahrt A., Neuhäuser R. 2007, MNRAS, 378, 1328

Neuhäuser R., Guenther E.W., 2004, A&A, 420, 647

Neuhäuser R., Guenther E.W., Wuchterl G. et al., 2005, A&A, 435, L13

Niedzielski A., Nowak G., Adamów M., Wolszczan A. 2009, arXiv: 0906.1804

Phan-Bao N. et al., 2008, MNRAS, 383, 831

Perryman M.A.C. et al., 1997, A&A, 323, L49

Pinfield D.J., Jones H.R.A., Lucas P.W. et al., 2006, MNRAS, 368, 1281

Pinfield D.J., Burningham B., Tamura M. et al., 2008, MNRAS, 390, 304

Radigan J. Lafrenière D., Jayawardhana R., Doyon R. 2008, ApJ, 689, 471

Radigan J., Lafrenière D., Jayawardhana R., Doyon R. 2009, ApJ, 698, 405

Ramírez I., Meléndez J., 2005, ApJ, 626, 465

Rebolo R., Zapatero Osorio M.R.Z., Martín E.L., 1995, Nature, 377, 129

Rebolo R., Zapatero Osorio M.R., Madruga S. et al., 1998, Science, 282, 1309

Reid I.N., Walkowicz L.M., 2006, PASP, 118, 671

Reid I.N., Cruz K.L., Kirkpatrick J.D. et al., 2008, AJ, 136, 1290

Ribas I., 2003, A&A, 400, 297

Röser S., Schilbach E., Schwan H. et al., 2008, A&A, 488, 401

Ruiz M.T., Leggett S.K., Allard F., 1997, ApJ, 491, L107

Salim S., Gould A. 2003, ApJ, 582, 1011

Schneider D.P., et al. 2002, AJ, 123, 458

Scholz R.D., McCaughrean M.J., Lodieu N., Kuhlbrodt B., 2003, A&A, 398, L29

Scholz Lodieu N., McCaughrean M.J. 2004, A&A, 428, L25

Seifahrt A., Guenther E., Neuhäuser, 2005a, A&A, 440, 967

Seifahrt A., Mugrauer M., Wiese M. et al., 2005b, AN, 326, 974

Sheppard S.S., Cushing M.C., 2009, AJ, 137, 304

Skrutskie M.F. et al., 2006, AJ, 131, 1163

Stoughton C. et al., 2002, AJ, 123, 485

Taylor B.J. 2006, AJ, 132, 2453

Tinney C.G., Delfosse X., Forveille T., 1997, ApJ, 490, L95

Tinney C.G., 1998, MNRAS, 296, L42

Tokovinin A., Thomas S., Sterzik M., Udry S., 2006, A&A, 450, 681

van Leeuwen F., 2007, A&A, 474, 653

van Leeuwen F., 2009, A&A, 497, 209

West A.A., Hawley S.L., Bochanski J. J., 2008, AJ, 135, 785

White R.J., Ghez A.M., Reid I.N., Schultz G., 1999, ApJ, 520, 811

Wilson J.C., Kirkpatrick J.D., Gizis J.E. et al., 2001, AJ, 122, 1989

Yi S., Demarque P., Kim Y.-C. et al., 2001, ApJS, 136, 417

York D.G. et al., 2000, AJ, 120, 1579

Zacharias N., Monet D.G., Levine S.E. et al., 2004, AAS, 205, 4815

Zacharias N. et al., 2009, yCat, 1315, 0

Zapatero Osorio M.R. et al., 1998, Brown dwarfs and extrasolar planets, P51

Zhang Z.H., Jones H.R.A., Pinfield D.J. et al., 2009a, Proceedings of the 10th Asian-Pacific Regional IAU Meeting 2008, P191, arXive: 0902.2677

Zhang Z.H. et al., 2009b, A&A, 497, 619

This paper has been typeset from a TEX/ LATEX file prepared by the author.